A Scaled Physical Model for Underwater Sound Radiation from a Partially Submerged Cylindrical Shell under Impact

A Thesis
Presented to
The Academic Faculty

By

Katherine F. Woolfe

In Partial Fulfillment
Of the Requirements for the Degree
Master of Science in Mechanical Engineering

Georgia Institute of Technology

August, 2012

A Scaled Physical Model for Underwater Sound Radiation from a Partially Submerged Cylindrical Shell Under Impact

Approved by:

Dr. Mardi C. Hastings, Advisor
The George W. Woodruff School of Mechanical Engineering
Georgia Institute of Technology

Dr. Aldo A. Ferri
The George W. Woodruff School of Mechanical Engineering
Georgia Institute of Technology

Dr. Erica E. Ryherd
The George W. Woodruff School of Mechanical Engineering
Georgia Institute of Technology

Date Approved: June 29, 2012

Acknowledgments

Throughout this thesis work, I have received help and encouragement from many people. First of all, I would like to convey my sincere gratitude to my advisor, Dr. Mardi Hastings, for her guidance, support, and encouragement. She has shown me what it takes to be a great scientist in the field of acoustics.

I would also like to thank my committee members, Dr. Erica Ryherd and Dr. Al Ferri, for their time to serve on my committee and their valuable insights to this thesis. Dr. F. Levent Degertekin also gave me valuable information regarding signal processing which was vital in analyzing the data in my experiment.

I would like to express my thanks to Jim Martin, Michael Gray, and Francois Guillot who have provided me with consistent help in setting up and testing equipment in the lab. Their knowledge, suggestions, and engineering skills have helped me to become a better experimentalist.

My sincere thanks to Shima Shahab for her insights into the structural acoustics of pile driving as well as her encouragement.

I must also convey special thanks to my husband, Chris Woolfe, for his patience, love, help getting me started with programming, and unfailing support. Many thanks as well to my parents, Jim and Barbara Faist, for their encouragement and love.

Finally and most importantly, I want to thank God, without whom I would not exist or have the ability to do this work at all.

Table of Contents

List of Tables

List of Figures

Summary

The motivation for this study is to create a scaled laboratory model of a steel construction pile being driven by an impact hammer, which can provide controlled data to aid understanding and development of a structural acoustics numerical model simulating full-scale impact pile driving. The scaled model is approximately thirty times shorter than a typical 30-meter long Cast-in-Shell-Steel (CISS) pile. The relationship between the impact force, structural vibrations, and radiated sound field is analyzed. The time-domain acoustic intensity in the radial direction is found to be predominately negative immediately following excitation by the impact force. Analysis of the radial intensity shows that during the hammer strike, there is a net flow of energy from the structure into the water; however, because the structure and water are acoustically coupled a significant portion of the energy immediately flows back into the cylinder following hammer impact. This fluid-structure interaction results in a highly damped acoustic pulse in the water that propagates to the far field. In addition, the frequency spectra of the impact force, model pile wall acceleration in the radial direction in air and water, and underwater acoustic pressure are analyzed to find transfer functions between these variables. The transfer function between impact force and sound pressure is of particular interest because it can be used to calculate the system response for any other applied hammer force. This transfer function analysis has potential applications in mitigating noise generated by impact pile driving.

Introduction

The high sound pressure levels that occur during pile driving can exceed 200 dB re 1 μPa at distances great than 100 m from the pile (Burgess, 2005). Levels this high can harm aquatic life that is protected by state or federal agencies (Popper and Hastings, 2009). To eventually mitigate the effects of these high sound pressure levels, research is being conducted to develop models to predict sound generated from submerged or partially submerged piles.

Previous Research

Only a few mathematical models have been proposed in the literature. A frequency-domain model developed by Hastings (2007) applies structural acoustic theory (Junger and Feit, 1993b) to a fully submerged, simply supported pile in a free field. Stokes *et al.* (2010) modeled a pile as an array of virtual sources when they examined wave propagation through air, water, and sediment following the hammer strike. Reinhall and Dahl (2011) attempted to correlate data generated from a virtual source model of a pile, treated as a phase array, to underwater sound pressure data collected during a pile driving test run at the Washington State Ferries (WSF) Vashon Island Ferry construction site. Recently, a finite-difference time-domain model was created by Hastings and Shahab (2012). While there are large amounts of underwater acoustic monitoring data from the field, these data are collected in uncontrolled environments and often under unknown conditions. This scarcity of reliable data makes it difficult to verify the various mathematical models that have recently been developed. This thesis documents the first

scaled physical model developed to investigate noise generated by a partially submerged pile under impact loading.

Objective

The objective of this research is to create a scaled physical model of pile driving in a laboratory setting which represents the field situation. This laboratory model will provide insight and data to correlate with the results of mathematical models in effort to develop methods to predict underwater sound propagation from impact pile driving.

Model Design and Analysis

This scaled physical model must be designed in such a way that the data collected from it is analogous to that from full-scale pile driving. The decreased size of the physical model generates higher resonance frequencies of the pile. Parameters that are important to measure in this model include the pressure at specific locations in the water, the wall motion of the pile, and the hammer force. Techniques that will be employed in the analysis of the data include transfer function analysis, cross correlation, and time-domain analysis. The time-domain analysis includes both direct analysis of the measured data and analysis of the energy exchange between structural vibrations and radiation of acoustic energy.

Overview

The motivation for this study is to design and test a scaled laboratory model of a steel pile being driven by an impact force. The scaled model is approximately thirty times shorter than a typical 30-meter long Cast-in-Shell-Steel (CISS) pile. The literature review cites

other sources that discuss the principles of model scaling, pile driving in the field, and calculations involving resonance frequency and energy transfer between the shell and the fluid. The experimental setup section describes the design of the laboratory model as well as the instrumentation used in this experiment. The results section details the relationships between radiated sound, pile wall motion, and impact force in both the time and the frequency domain for the scaled model. This analysis ultimately provides a better understanding of the fluid-structure coupling in the time domain, and the transfer function between input force and acoustic pressure can be used in the future to investigate force waveforms that have potential to reduce radiation of acoustic energy to the far field.

Literature Review

Impact Pile Driving: an Overview

Figure 1: Impact pile driving of a 30”-diameter, partially submerged CISS pile at the Friday Harbor Ferry Terminal on San Juan Island (Carlson and Weiland, 2007)

Cast-in-Shell-Steel (CISS) piles are typically used to support structures such as bridges, piers, and offshore platforms. These piles can vary in length from 10 m to 100 m. There are several methods that are currently used to hammer the piles into the sediment. The method that is studied here is the use of an impact hammer. Impact hammers are dropped on top of the pile. Diesel or hydraulic power is often used to assist lifting the hammer to the height needed to provide enough energy to penetrate the sediment (ICF Jones & Stokes and Illingworth and Rodkin, Inc., 2009) . The hammer generates a transient force

at the top of the pile, driving the pile downwards into the sediment. During the pile driving process, dynamic measurements of the pile wall are made to adjust the impact force to ensure structural integrity and prevent buckling.

During pile construction, peak sound pressure levels can exceed 200 dB (re 1 μPa) 10 m from the pile for a 96-inch diameter CISS pile (ICF Jones & Stokes and Illingworth and Rodkin, Inc., 2009). These high sound pressure levels coupled with high particle velocities have been demonstrated to have adverse effects on aquatic life. These adverse effects include changes in behavioral patterns, damage to internal tissues, and even death (Popper and Hastings, 2009). Techniques to mitigate acoustic impacts from pile driving noise include bubble curtains, dewatered cofferdams, and encapsulation of the pile with foam; however, these methods are costly and have limited effectiveness (ICF Jones & Stokes and Illingworth and Rodkin, Inc., 2009).

Transducer Setup in Field

The American Society for Testing and Materials (ASTM) D4945 (2008) standard specifies dynamic testing of piles in the field. These measurements are taken with transducers mounted on the external surface of the pile wall. The recommended test setup is shown in Figure 2. It is important to know the transducers that are used in the field to design an approximate physical model, especially if the results from this study are to be applied to full-scale piling activities.

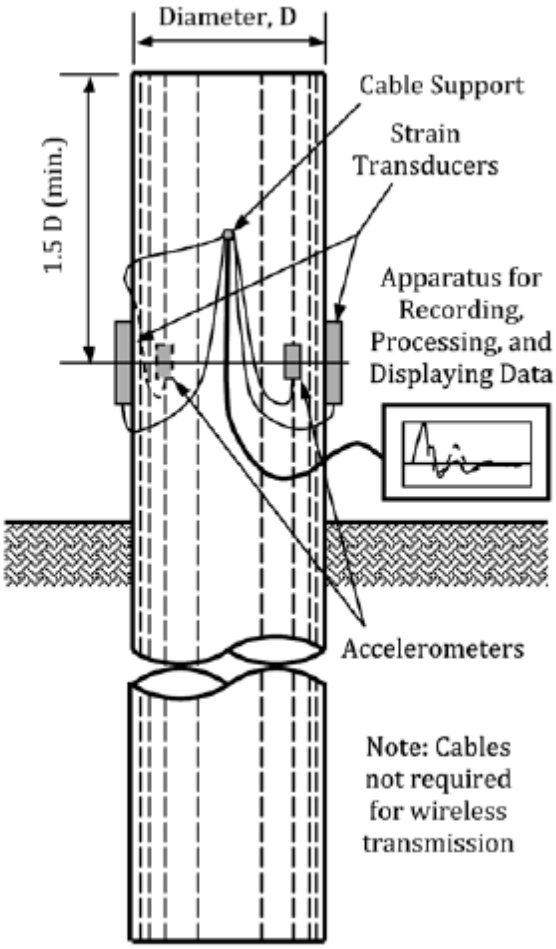

Figure 2: Standard Pile Monitoring in the Field (adopted from ASTM D4945, 2008)

The wall-motion transducers are mounted at a minimum distance of 1.5 diameters from the top of the pile. These transducers include both accelerometers and strain gauges. The strain gauges measure the axial strain along the pile, and the accelerometers measure motion in the radial direction. The strain gauges and accelerometers are oriented around the pile in a symmetric fashion so as to cancel out strain and moments due to bending.

Prediction of Resonance Frequencies

Prediction of the primary resonance frequencies for a given pile is crucial in the process of scaling down from a full-scale pile to the laboratory model. When the hammer hits the pile, many modes are excited in the longitudinal, circumferential, and radial directions. Since radial modes are the ones that couple directly to the water to create sound waves, these are the ones that will be investigated. Because of relatively high radiation damping underwater, which increases with frequency, pile noise is generally in the low- to mid-frequency range. The cutoff between the mid- and high-frequency ranges is defined to be when the ratio of circumference to wavelength equals five (Junger and Feit, 1993b). Thus frequencies above this cutoff are not analyzed.

The assumption that the pile is simply supported is a fair approximation of the pile cap at the top end and the sea bed at the bottom end, which restrict motion in the radial and circumferential directions, but allow for motion in the axial direction. The dimensionless natural frequencies, Ω_{mn}, for predominately radial modes of a fully submerged, simply supported shell are given by (Junger and Feit, 1993b):

$$\Omega_{mn} = \frac{[(1-\upsilon^2)(k_m a / k_s a)^4 + \beta^2 k_s{}^4 a^4]^{1/2}}{[1+n^{-2}+(\rho/\rho_s k_s h)]^{1/2}} \qquad \textbf{(1)}$$

where Ω_{mn} is the dimensionless natural frequency, defined by $\Omega_{mn} = \omega a/c_p$, where ω is the radial frequency in radians per second, c_p is the phase velocity of compressional waves in meters per second, a is the internal radius of the cylinder, and $\beta^2 = h^2/(12a^2)$. m and n are the mode numbers in the longitudinal and circumferential directions, respectively, υ is the Poisson ratio of the shell, h is the wall thickness in meters, $k_s = (k_m{}^2 + n^2/a^2)^{1/2}$, ρ is the density of water, and ρ_s is the density of the shell. For these radial modes, $k_m = m\pi/L$

(*m=1,2,3…).* These natural frequencies are computed assuming linear elastic deformation, *h/a<<1*, and small radial displacements compared to shell thickness. It must be noted that this equation for modal frequencies was derived for submerged cylindrical shells filled with air. However, since work conducted by Gonçalves and Batista (1987) demonstrates that natural frequencies of a submerged and fluid-filled shell are only slightly lower than those of a submerged air-filled shell, this equation is deemed to be a close enough approximation of the natural frequencies of a fully submerged or partially submerged pile.

Physical Model Scaling and Similitude

Perhaps the single most important consideration in the planning and evaluation of physical model experiments in underwater acoustics is that the physical apparatus is not an exact scale model of the underwater field environment. Hydroacoustic models inevitably involve physical quantities, such as fluid properties like viscosity and absorption, which are not scaled. On the other hand, because of the reduced dimensions of the model, the acoustic wavelength scale is reduced. This results in a relationship between field phenomena and those observed in a physical model that is more complex than a simple scaling factor. This relationship, however, can be accounted for in a mathematical model by appropriately adjusting the physical dimensions and boundary conditions for the scaled model. Then a scaled physical model can be used to verify the mathematical model.

When the assumptions are equally valid in both the mathematical model and physical model, the physical model's dimensions are driven by a frequency scaling factor (Zornig, 1979). The assumptions for the pile scaled model considered here are as follows:

1. The pile is approximated as a simply supported cylindrical shell.
2. The pile has constant wall thickness.
3. Thin shell theory is defined as the pile wall thickness being less than 10% of the pile radius. (Junger and Feit, 1993a)
4. The pile is composed of a linear, elastic, homogenous, and isotropic material.
5. The pile is not pre-loaded.
6. Water viscosity is neglected
7. Rotational inertia and shear deformation are neglected.
8. All pile deformations are small and therefore linear.
9. The aspect ratio (L/a) is large.
10. Frequencies emitted by the pile are in the low-frequency to mid-frequency range, where the ratio of circumference to wavelength is less than five (Junger and Feit, 1993b).

Scaling laws for structural acoustics were recently considered by De Rosa *et al*. (2012) and Wang *et al*. (2007). Wang *et al*. consider effects that may be present in a small model that are not present in a full-scale model, such as viscosity and boundary effects. De Rosa *et al*. also assert that to achieve complete acoustic similitude (i.e., perfect scaling), it is necessary to not just scale by frequency, but also maintain the same wall thickness-to-

radius and aspect ratios. In this study, the aspect ratio could not be appropriately scaled in the physical model due to the geometrical limitations of the laboratory and available pipe geometries. The difference in aspect ratio will be discussed in detail in the experimental setup section. Boundary conditions imposed by the laboratory shallow water tank will have an effect on the underwater acoustic intensity in the circumferential and longitudinal directions. This will be discussed in detail in the results section. Viscosity effects are still deemed to be negligible.

Effects of Water Height on Sound Radiation from a Submerged Pile

While the vibrations of shells in air differ little from the vibrations of shells in a vacuum, this is not the case for a cylindrical shell that is fully or partially submerged in a liquid (Junger and Feit, 1993b) The lowest natural frequency of a shell in water is much less than the lowest natural frequency of a shell in air. This frequency is highly dependent on the liquid level and mode shapes and physical dimensions of the shell. The radiation loading exerted by the surrounding fluid on the shell modifies the structural vibrations of the cylinder, and the structural vibrations, in turn, change the radiation loading, resulting in a coupling effect. The natural frequency of a shell decreases as the percent of the shell that is submerged increases. These effects are examined in detail by Gonçalves and Batista (1987).

Determining Energy Exchange at a Surface

Extensive theoretical and experimental work has focused on understanding the fluid-structure interaction for acoustic radiation from submerged, vibrating bodies. Most

previous analysis has been confined to the frequency domain and the acoustic far field. The development of near-field acoustical holography (NAH) allowed determination of energy radiated to the far field by measurement of a structure's vibrational energy and acoustic energy in the near field (Mann *et al*. 1991). By applying a linear system model, a single input-output transfer function, $h(\tau,r,z)$, can be determined between the drive force, $f(t)$, and a field quantity, $y(t,r,z)$, at a given point in the fluid for a submerged cylindrical shell with axisymmetric loading. Candidates for the field quantities include the acoustic pressure or particle velocity at a position in the fluid due to the force on the shell. In this case, pressure is used as the field quantity.

To obtain the transfer function, first the complex acoustic pressure over a cylindrical surface enclosing the shell is measured simultaneously with the drive force excitation. Then a Fast Fourier Transform (FFT) is performed on the time-domain input force and the field quantity at each measurement location. In the frequency domain, the relationship between the drive force and the field quantity can be expressed as a multiplication, assuming a linear system model:

$$y(\omega ,r, z)= h(\omega ,r, z) f(\omega) \qquad \textbf{(2)}$$

By dividing $y(\omega ,r, z)$ by $f(\omega)$ at each measurement location, the transfer function, $h(\omega,r,z)$, is easily obtained. This gives the impulse response spectra for the pressure at every location on the measurement surface. These impulse response spectra enable one to find the field quantity, in both the time and frequency domain, at a specific point for any force input.

It is also useful to examine the energy exchange between the cylindrical shell and the fluid. First, it is important to consider a fundamental power balance formulation (Mann *et al.* 1991). The total change in energy within a volume, *V*, is expressed as an integral of the instantaneous intensity over a surface enclosing the volume. In integral form this is expressed as:

$$\frac{\partial}{\partial t}\iiint_V \left[\boldsymbol{E_k}(\boldsymbol{t},\boldsymbol{r},\boldsymbol{z}) + \boldsymbol{E_p}(\boldsymbol{t},\boldsymbol{r},\boldsymbol{z})\right]\boldsymbol{dV} = -\iint_S \boldsymbol{I_n}(\boldsymbol{t},\boldsymbol{r},\boldsymbol{z})\boldsymbol{dS} \qquad \textbf{(3)}$$

where $E_k(t,x)$ is the kinetic energy, $E_p(t,x)$ is the potential energy, and $I_n(t,x)$ is the instantaneous acoustic intensity normal to the surface *S*, where *S* is the surface enclosing the volume and is close to the surface of the shell. $I_n(t,x)$ can be determined experimentally, and then the right-hand side of the equation can be calculated. The surface integral is approximated with a spatial sum over all data points of the instantaneous intensity at each time step. The surface integral is equivalent to the total change of energy in the volume. If the instantaneous normal intensity is positive, then the measurement surface injects energy into the fluid. If the instantaneous normal intensity is negative, then the fluid injects energy back into the measurement surface. To find the total amount of energy in the volume, Equation (3) is integrated with respect to time, resulting in Equation (4):

$$\iiint_V \left[\boldsymbol{E_k}(\boldsymbol{t},\boldsymbol{x}) + \boldsymbol{E_p}(\boldsymbol{t},\boldsymbol{x})\right]\boldsymbol{dV} = -\int_{-\infty}^{\boldsymbol{t}} \left(\iint_S \boldsymbol{I_n}(\boldsymbol{\tau},\boldsymbol{x})\boldsymbol{dS}\right)\boldsymbol{d\tau} \qquad \textbf{(4)}$$

The right-hand side of Equation (4) is calculated by discretely integrating the previously calculated right-hand side of Equation (3) over time. This represents at each time, *t*, the total energy which has passed through the measurement surface into the fluid.

Experimental Setup

Normal Modes of the Test Tank

A picture of the test tank is shown in Figure 3. The taller pipe in the tank is the model pile used in this experiment, and its end caps are adjacent to it on the bottom of the tank.

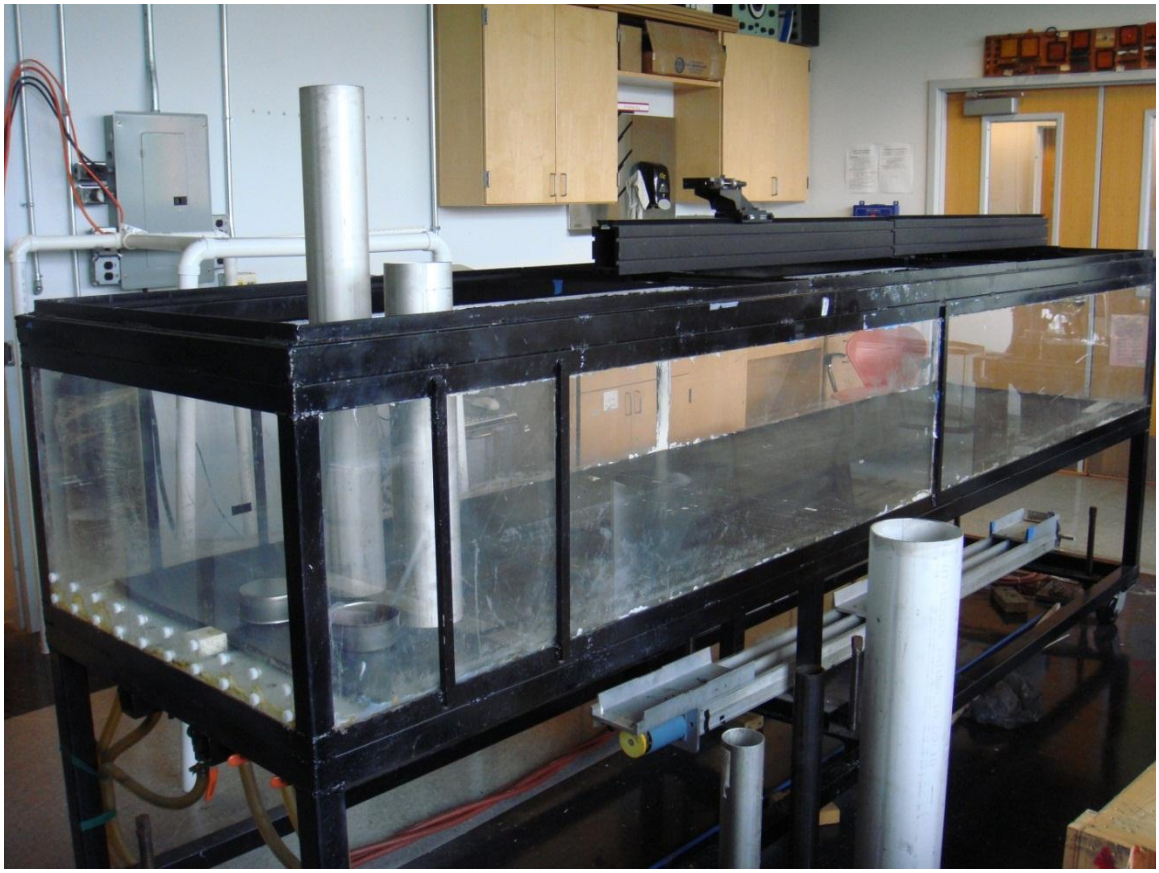

Figure 3: The tank and the pile used in this experiment. The model pile is the taller one in the tank.

The dimensions L_x, L_y, and L_z of the test tank are shown in Figure 4.

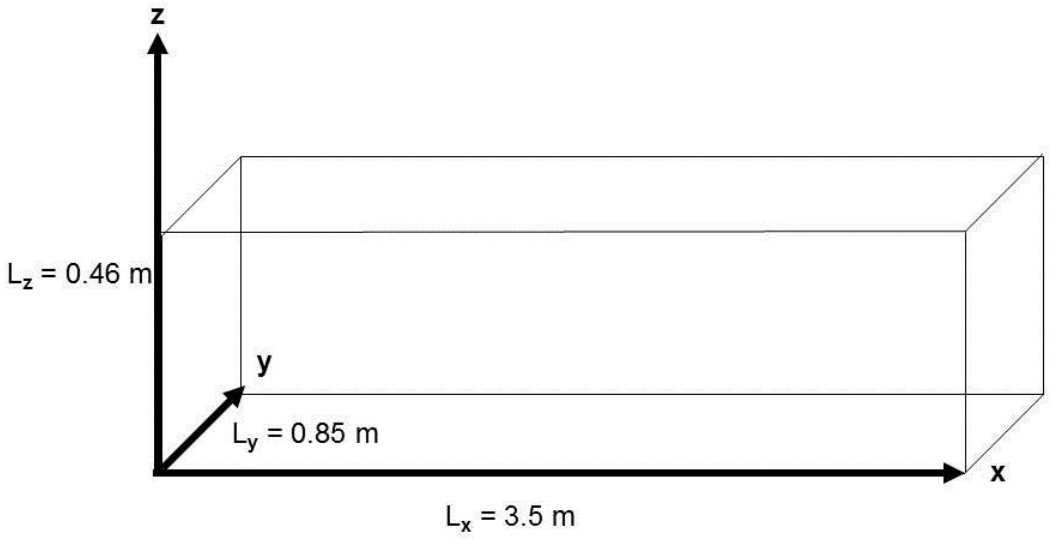

Figure 4: Test Tank Dimensions

The normal modes of the tank identify frequencies that could be amplified due to resonance. Before calculating these frequencies, certain simplifying assumptions are made about the tank environment. The bottom of the tank is covered by 0.01 m thick neoprene rubber with a sound speed of 1490 m/s and a density of 960 kg/m^3 (Yang, 2007). Because this rubber has a characteristic impedance that is close to that of water, it is ignored for the calculation of the modal frequencies of the test tank. The glass walls and bottom of the tank are assumed to be rigid for the purposes of these calculations so that the normal component of the particle velocity vanishes at those boundaries. Although this approximation is not exact, it is reasonable enough to provide a general idea of the range of frequencies that would cause resonance in the tank. The water surface, located at z=0.46 m, is a pressure release surface. The modal wave numbers in the x, y, and z directions are given below as functions of the mode numbers: l, m, and n.

$$k_{xl} = (\pi l)/L_x \quad \textbf{(5)}$$

$$k_{ym} = (\pi m)/L_y \quad \textbf{(6)}$$

$$k_{zn} = (2n+1)\,\pi/(2L_z) \quad \textbf{(7)}$$

Combining the wave numbers in all three directions yields the total wave number. This is used to calculate the modal frequencies:

$$f_{lmn} = \frac{c\sqrt{k_{xl}^2 + k_{ym}^2 + k_{zn}^2}}{2\pi} \quad \textbf{(8)}$$

The ten lowest non-degenerate modal frequencies are shown in Table 1. The transient nature of the impact force means that it is unlikely for these normal standing modes to have enough time to fully develop, since normal modes are determined using continuous wave analysis.

Table 1: Ten lowest non-degenerate normal modes of the tank

l	**m**	**n**	**f_{lmn} (Hz)**
1	0	0	830
0	1	0	1185
0	0	1	2413
1	1	0	1200
0	1	1	2565
1	0	1	2422
1	1	1	2574
2	0	0	908
0	2	0	1918
0	0	2	4022

Frequency Scaling to Determine Model Pile Dimensions

Selection of the model pile depends primarily on the frequency scaling between a full-size pile and the model. The full-size pile and the model are both steel. There are many sizes of piles that are commonly used, with diameters ranging from 1 ft to 12 ft (ICF Jones & Stokes and Illingworth and Rodkin, Inc., 2009). Each size pile emits a different range of frequencies. Piles that are useful to compare to the scale model are listed in Table 2. The smaller dimensions of the scaled pile result in higher resonance frequencies. Equation (1) is used to predict the modal frequencies emitted by the scaled pile. Equation (1) is only valid for predominately radial modes where $n > 0$. As discussed previously, Equation (1) is an approximation that is used to calculate the primary resonance frequency for a fully submerged cylindrical shell. However, the model pile is partially submerged. Partially submerging the shell will increase the calculated resonance frequency (Gonçalves and Batista, 1987).

Table 2 tabulates the predicted lowest modal frequency (m=1, n=1) and checks the assumptions for the selected stainless steel scaled pile with a nominal diameter of 0.11 m, assuming a sound speed in steel of 5.24×10^3 m/s and a sound speed in fresh water at 20 °C of 1480 m/s. The $f_{m,1}$ modes are all axisymmetric (with a single lobe in the circumferential direction) and predominately radial. The water depth in the test tank is 0.46 m..

Table 2: Scaled pile characteristics compared to full-size pile characteristics (Using fully submerged approximation)

Pile Nominal Diameter (m)	Pile Length (m)	$f_{1,1}$ (Hz)	L/a	h/a	circum. / λ (in water)	Upper Frequency Bound (kHz)
0.11 (4.5")	0.91	1700	17	0.06	0.41	21
0.61 (24")	30	45	110	0.09	0.06	3.9
0.91 (36")	30	23	70	0.06	0.04	2.6
1.52 (60")	30	23	41	0.03	0.07	1.6
2.40 (96")	30	29	25	0.02	0.15	0.9

The upper frequency bound for the prediction equations to hold is determined from the assumption that the frequencies emitted by the pile must be in the low- to mid-frequency range. When the ratio of circumference to wavelength is greater than five (Junger and Feit, 1993b), then these frequencies are too high for the analysis to hold. For the model pile, the demarcation between the mid- and high-frequencies occurs at 21 kHz. For frequencies greater than 21 kHz for the model pile, high frequency analysis must be used, and the analysis for low to mid frequencies will not apply. Low- to mid-frequencies analysis applies to partially and fully submerged cylindrical shells because of relatively high radiation damping in water.

As a result of this frequency analysis, a steel cylinder 0.91-m in length, with a 3-mm wall thickness and a 0.11-m diameter was chosen for the scaled model pile. Because the water depth is held constant at 0.46 m, this model pile is partially submerged. This is the maximum water depth that is achievable in the test tank; however, these resonance frequency predictions allow for a general scaling factor of around 40. This scaling factor was used to place hydrophones in

the model at positions that correlate to measurement locations that are commonly used in the field.

An obvious discrepancy is the change in aspect ratio. While it is ideal to maintain a constant aspect ratio, it was necessary to decrease the aspect ratio of the model pile because of the constraints of the tank and room dimensions and the available pipe diameter. This is explained in Table 3.

Table 3: Demonstration of how the laboratory physical limitations limit the model pile aspect ratio (aspect ratio for 96" pile is 25, *h/a*= 0.02)

Standard pipe size (in.)	Wall Thickness (mm)	Outer Diameter (m)	L_{max} from physical limits (m)	Max. aspect ratio (*L/a*)	*h/a* (needs to be <<1 for thin shell)
4, Schedule 10	3 (0.1")	0.11 (4.5")	0.91 (36")	17	0.06
3, Schedule 10	3 (0.1")	0.09 (3.5")	0.91 (36")	22	0.07
5, Schedule 5	3 (0.1")	0.14 (5.6")	0.91 (36")	13	0.04

Instrumentation

The instrumentation used in the experiment is shown in Figure 5. The 3-D automatic positioning system moves the hydrophones to enable measurement of pressure gradients. The three RION PV08A accelerometers measure the wall motion of the cylindrical shell in air. The mini impulse hammer was chosen because of its frequency response characteristics, generating frequencies up to 30 kHz. In addition, a PDV 100 laser is used to measure the surface velocity in the radial direction at a point 0.30 m from the bottom of the pile, which is in the submerged portion of the model.

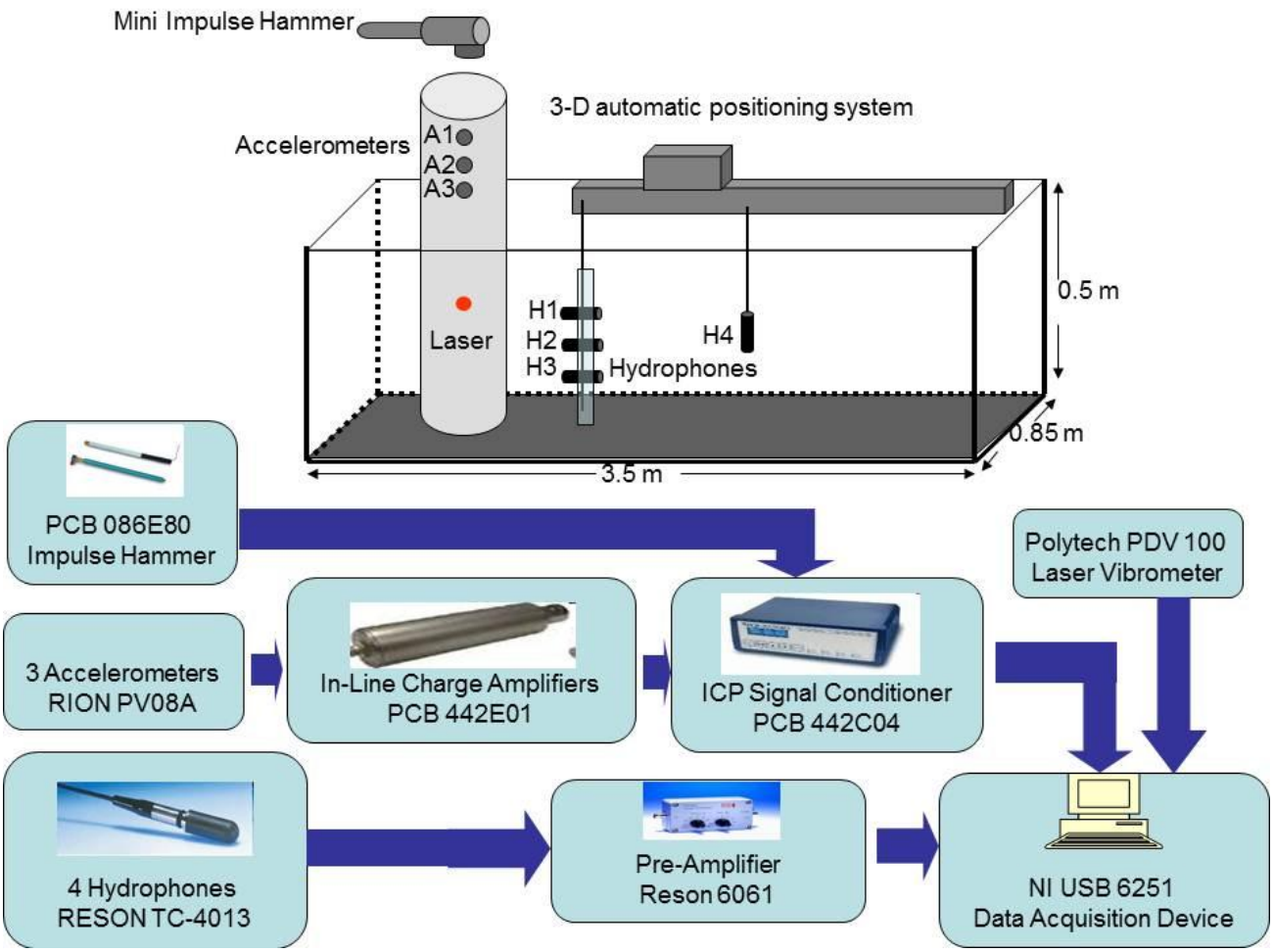

Figure 5: Instrumentation for the partially submerged scale model experiment (figure is not to scale)

The serial numbers and sensitivities of all sensing devices are shown in Table 4.

Both the hydrophones and the accelerometers are numbered from the top to the bottom of their respective positioning lines (i.e H1 is the top hydrophone; H2 is the middle one, etc.).

Table 4: Instrumentation Details

Sensing Device	Serial Number	Sensitivity	Manufacturer
Hydrophone 1 (TC4013)	1611198	-211 dB re 1V/μPa	Reson
Hydrophone 2 (TC4013)	1611216	-211 dB re 1V/μPa	Reson
Hydrophone 3 (TC4013)	1611210	-211 dB re 1V/μPa	Reson
Hydrophone 4 (TC4013)	1611216	-211 dB re 1V/μPa	Reson
Impact Hammer (PCB 086E80)	30076	23.42 mV/N	PCB
Accelerometer 1 (PV-08A)	11854	0.098 pC/(m/s^2)	Rion
Accelerometer 2 (PV-08A)	11855	0.098 pC/(m/s^2)	Rion
Accelerometer 3 (PV-08A)	11856	0.099 pC/(m/s^2)	Rion
Laser (PDV 100)	0113268	25 (mm/s)/V	Polytech

Laser Vibrometer Analysis

The Polytech PDV 100 laser vibrometer is used to measure the outer wall radial velocity of the pile at a location that is underwater. The data collected by the laser will provide insight into how the fluid loading affects the model pile wall motion. The laser is positioned on the outside of the tank so that the beam is normal to the glass tank wall. The beam passes through the air, glass, and water before hitting the primary reflector of the model pile outside wall. The theoretical development of the use of a laser vibrometer to measure the vibrations of an underwater object is detailed by Marsili *et al*. (2000). When an object surface vibrates inside a still fluid with a refractive index n_{fluid}, the measured voltage from the laser vibrometer needs to be divided by n_{fluid}

as a correction factor. Because the refractive index of water is 1.33, voltage measurements need to be divided by 1.33 to attain the correct values.

Hydrophone Placement

The hydrophones used in this experiment are positioned in a vertical configuration in the near-field. The demarcation for the end of the near field was estimated to be ten wavelengths of the highest frequency to be measured for the pile. The highest frequency is approximately 21 kHz, as seen in Table 2. Using a sound speed of 1480 m/s in water, ten wavelengths at the highest frequency is equal to a distance of 0.7 m. Three Reson 4013 hydrophones are arranged in one vertical line at a distance of 0.34 meters from the pile outside wall in the near field. Because a broad range of frequencies are emitted by the pile, there is a large distance of transition from near field to far field in the tank. The distance from the pile to the far field is equal to ten wavelengths of the lowest frequency, which is approximately 1.7 kHz. This corresponds to a distance of 8.7 meters, which is much longer than the length of the tank. A fourth hydrophone is positioned along the center axis at 0.94 m from the pile axis as shown in Figure 6. This is located in the transition from near field to far field. The hydrophones are actuated by a 3-D positioning system in order to measure the pressure gradient at three points along a line parallel to the longitudinal axis of the pile as illustrated in Figure 7.

Each single hydrophone is actuated to 9 different locations defined as the vertices and center of a cube with sides 1 cm long. These measurements allow for the calculation of particle velocity vectors at each hydrophone location through the use of Euler's equation of motion:

$$\boldsymbol{\rho_0 \frac{\partial \vec{u}}{\partial t} = -\nabla p} \tag{9}$$

Once the particle velocity vectors are calculated, the instantaneous acoustic intensity vectors are found by multiplying pressure and particle velocity.

$$\boldsymbol{\vec{I} = p\vec{u}} \tag{10}$$

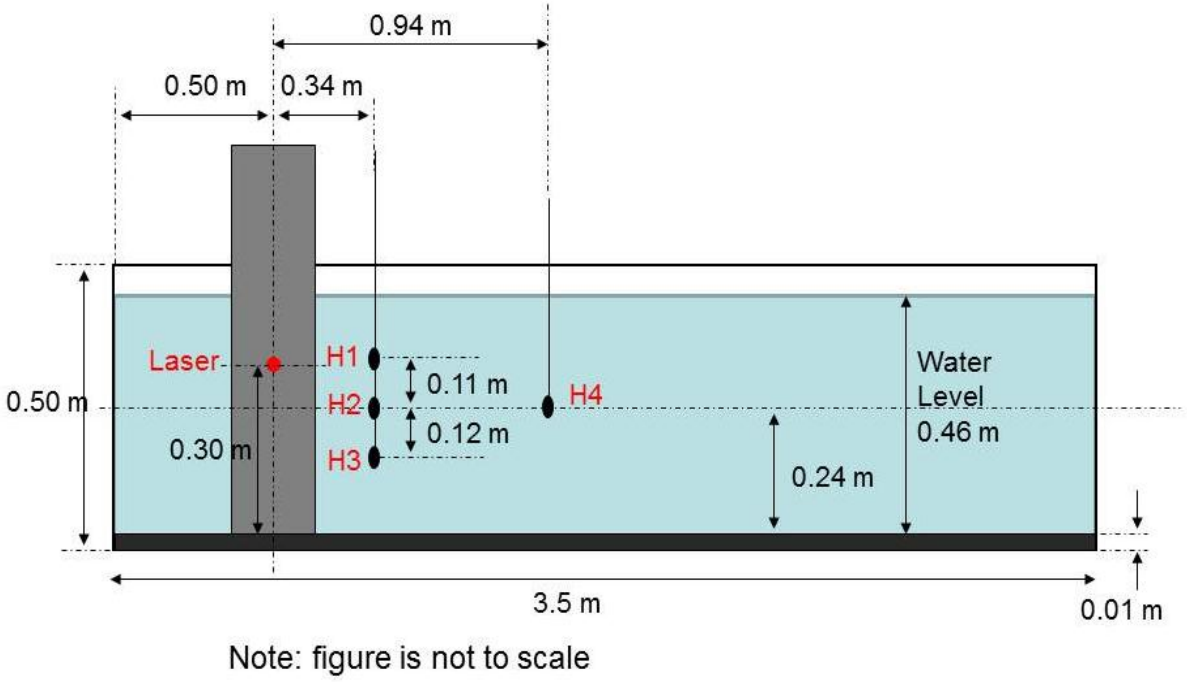

Figure 6: Schematic of the hydrophone locations

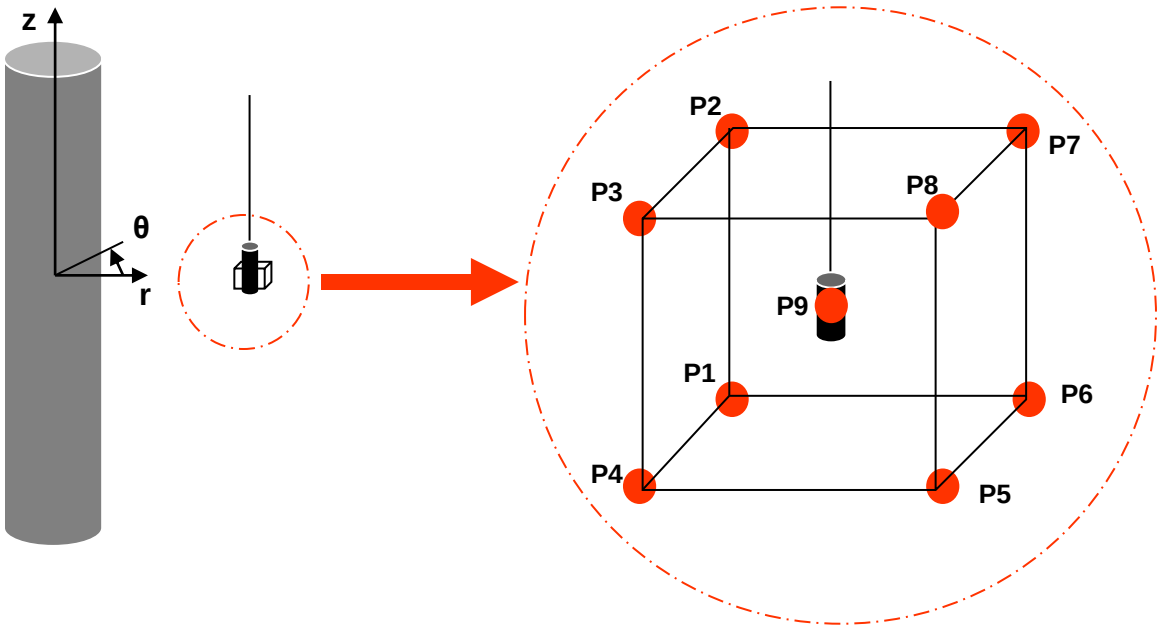

Figure 7: Measurement positions for a single hydrophone

Accelerometer Placement

Three Rion PV-08A accelerometers are placed on the outside wall of the pile in air. Because the hammer strikes the center of the pile cap, it is reasonable to assume axisymmetric vibrations. As a result, the accelerometers are placed in a line parallel to the longitudinal axis of the pile. The exact placement of the accelerometers was chosen to be far enough away from the pile cap to reduce the effects of the boundary conditions, but still far from the water surface. Accelerometers 1, 2, and 3 are located 0.05 m, 0.07 m, and 0.09 m, respectively, from the top of the pile.

Hammer Drop Mechanism

The force input to the model pile system is provided by a PCB 086E80 miniature impulse response hammer. The hammer is attached to a pivot arm, which pivots via a greased bearing

supported by an aluminum frame. The pivot arm is manually released from an angle of approximately 60 degrees, shown in Figure 8. Upon release, the hammer pivots about the bearing while it swings downward. The tip of the hammer impacts the center of the pile cap. This design was chosen to simulate the drop of a field impact hammer. Because the laboratory physical constraints prevented the hammer descending in a vertical line onto the pile cap, a pivot arm was chosen instead. Care was taken to ensure that the tip of the hammer was applied normal to the surface of the pile cap.

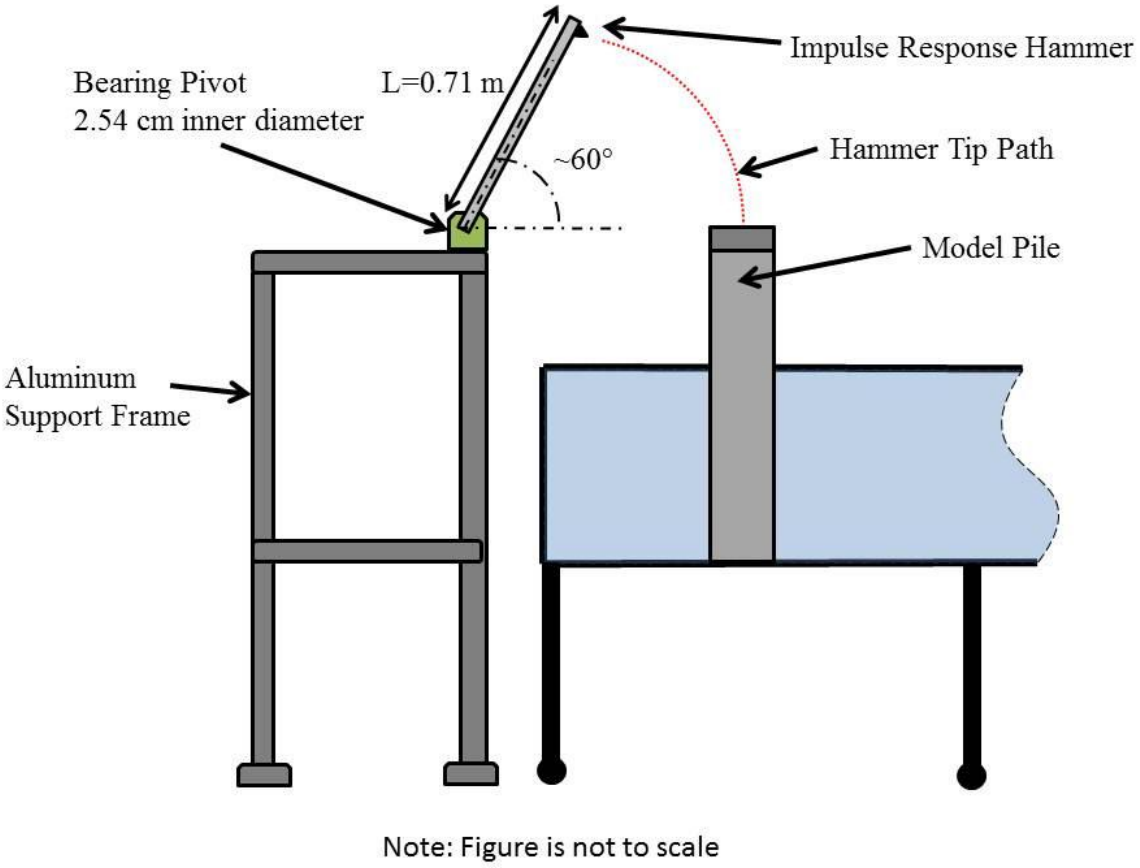

Figure 8: Hammer frame and arm setup. The hammer is manually released from approximately 60 degrees and pivots about the bearing until it impacts the center of the model pile cap. This figure is not to scale.

Description of Measurement Methodology

At the beginning of each day of data collection, the water level and water temperature in the test tank was measured. The accelerometers were hot glued onto the outside wall of the model pile. Care was taken to ensure that the accelerometers were positioned normal to the wall of the pile to measure radial acceleration. The impact hammer was attached to a pivot arm that was manually released from a starting position. The hammer tip would strike the pile vertically in the middle of the top end cap. The PDV 100 laser was positioned on a tripod adjacent to the water tank. The laser beam was placed so that it was normal to the glass tank wall and normal to the pile wall.

The automated positioning system was used to position all the hydrophones so that each hydrophone would be at the same measurement position number in its own measurement cube (see Figure 7). With each hydrophone positioned in the same position number, the data collection would begin. After the start of the data collection, the hammer was manually dropped onto the top end cap of the model pile. Care was taken to ensure consistency in the hammer drops, but the hammer drop is still influenced by human error. For each hammer drop, sound pressure at all four hydrophones, acceleration at all three accelerometers, hammer force, and laser data were all collected at a sampling rate of 100 kHz over a total time of three seconds. This process was repeated nine times per measurement position. There are nine measurement positions. For each measurement position, the data collected over ten hammer drops was averaged. Underwater background noise was also measured on several different days to establish a cutoff for meaningful sound pressure data.

Data Analysis

To understand the relationship between impact force and the radiated acoustic field, it is necessary to find the transfer function between impact force and field variables. For this experiment, transfer functions are found between impact force and pressures measured by hydrophones 1, 2, and 3. Additionally, a transfer function is found between radial wall acceleration and pressure measured by hydrophone 2 to examine the effect of the fluid-structure interface on wave propagation. Instantaneous intensity vectors are used to understand the flow of energy through an imaginary surface surrounding the pile. This gives insight into how the structure and the fluid exchange energy in the time domain.

Negligible Reflection Effects

Because the pressure data collected are all derived from a highly damped transient impact event and the sound pressure is also highly attenuated in water, the effects of reflections off the tank walls are considered to be negligible. Therefore, all measured data in the time domain is considered useful for analysis. However, reflections off the water surface and the neoprene at the bottom do affect the calculated intensity in the vertical direction.

Background Sound Pressure Measurements

The background noise from 0.5 kHz to 20 kHz is shown in Figure 9. These data were measured by hydrophone 2 at a sampling rate of 100 kHz and a water temperature of 17°C .

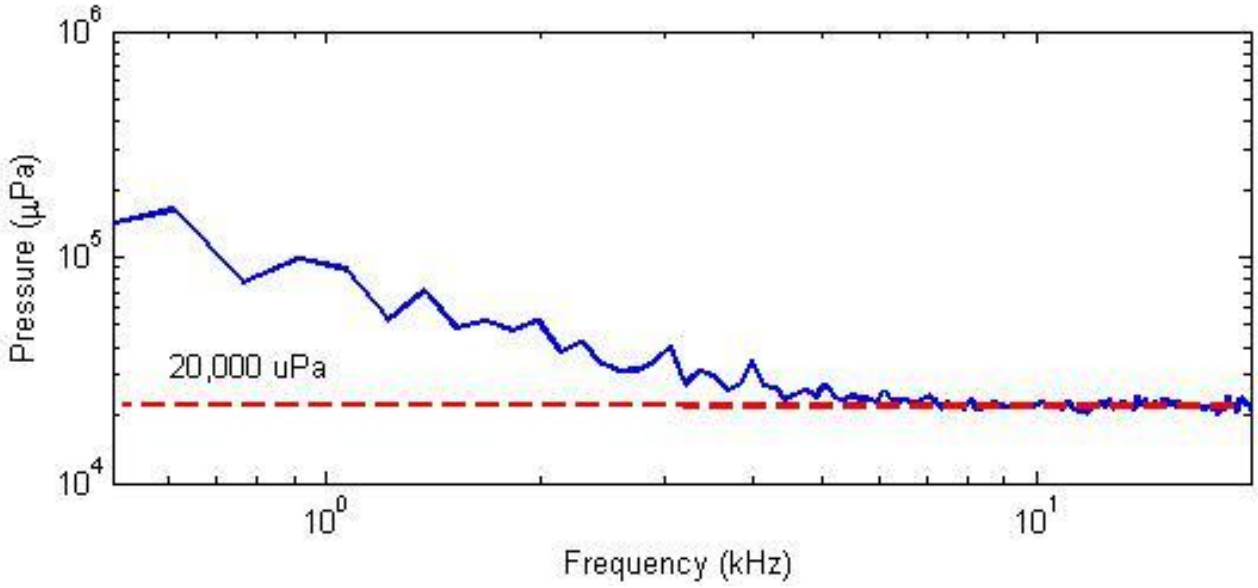

Figure 9: Background sound pressure spectrum in the test tank over 150 Hz bands

It is important to characterize this background noise to establish a cutoff criterion for the measured signal. The time domain data is zero padded to achieve an array length of the next power of two. After the Fast Fourier Transform (FFT) is performed, the data is normalized by dividing by the number of data points, and then the data is squared to get the power spectral density. The data above the Nyquist frequency of 50 kHz is dropped, and the data below the Nyquist frequency is multiplied by two to keep the same energy in the signal. The DC component and the Nyquist component are both unique and therefore are not multiplied by two. Discretely integrating the power spectral density over bands of 150 Hz yields the sound pressure squared. Applying a square root to the squared data gives the sound pressure. This bandwidth

was necessary to visualize the data, although a narrower band would help to better distinguish individual peaks in the spectra.

Signal Arrivals

The data collected in the time domain are shown in Figure 10. This figure shows the relative signal arrival times for the impact force, accelerometer 1, hydrophone 2, laser, and hydrophone 4. This is only plotted for the first 3 milliseconds to look at the signal arrival times. One obvious issue that should be discussed here is the delay in signal arrival for the laser. Theoretically, the laser signal arrival time should be only slightly after the accelerometer signal arrival. This large measured delay is due to the internal processing of the laser, as shown in the PDV 100 manual, and therefore the laser data will primarily be analyzed in the frequency domain (Polytech 2001). The delay between signal arrivals at hydrophone 2 and hydrophone 4 is approximately 0.4 ms. These hydrophones are separated by a distance of 0.6 m, and applying a sound speed of 1480 m/s gives 0.41 ms as the predicted delay. This check shows that other than the laser arrival time, the rest of the arrivals are as expected.

Force and Pressure

The impact force applied by the 086E80 impulse response hammer is shown in Figure 11. It can be seen that the first portion of the impact force occurs over 2 ms. The second portion of the impact force is due to a hammer bounce, which creates a similar waveform of decreased amplitude. The impact force reaches a peak of approximately 400 N and is averaged over 10 hammer drops per measurement location. Given 9 measurement locations, the figure below plots the force profile averaged over 90 total runs. The standard deviation of the measured force is

also plotted. Because the hammer was released manually, a large amount of practice and effort was involved in minimizing the standard deviation of the hammer waveform. In all time-domain plots, zero time coincides with the beginning of the hammer strike. The frequency content of the hammer signal is shown in Figure 12. These data are weighted in the frequency domain by the hammer frequency response curve shown in the appendix. It is important to determine the frequencies that are put into the pile and water system by the hammer to characterize the transformative effects (if any) of the system in the frequency domain. The predominant frequencies transmitted to the system by the hammer are around 1.5 kHz and 4 kHz. These data are filtered by a high pass, fourth order Butterworth filter with a cutoff frequency of 500 Hz.

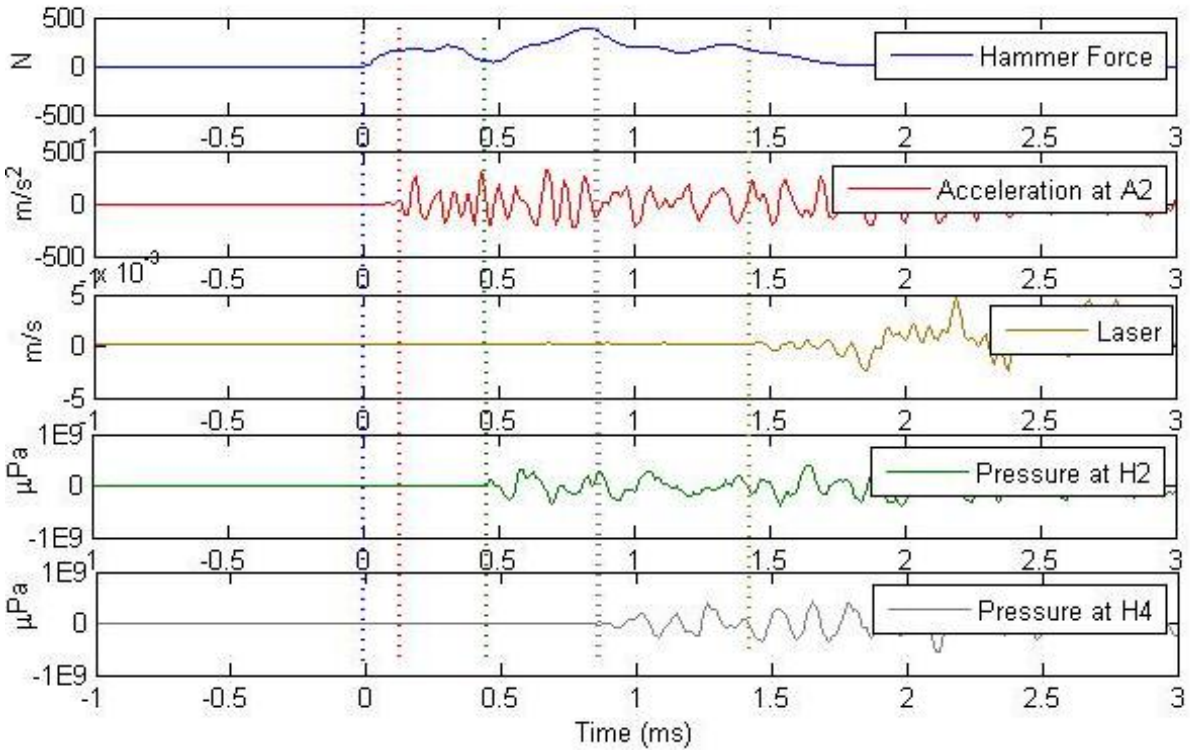

Figure 10: Signal arrivals with each arrival marked by a dotted line

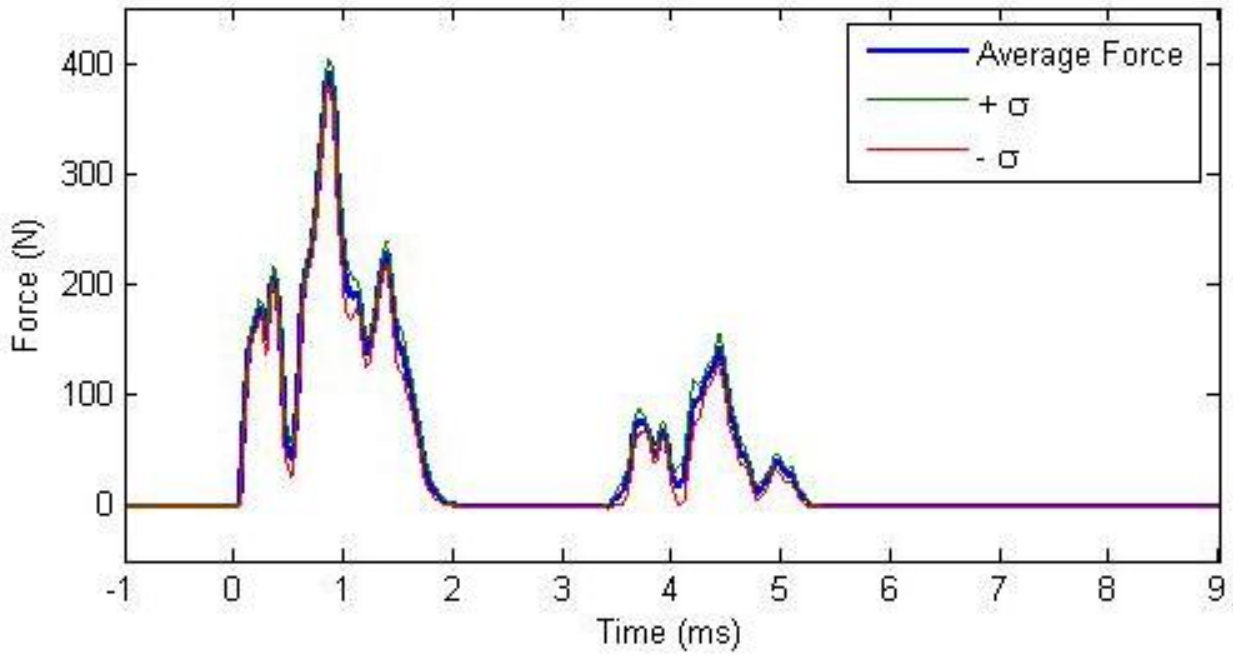

Figure 11: Force applied by the impact hammer to the pile top

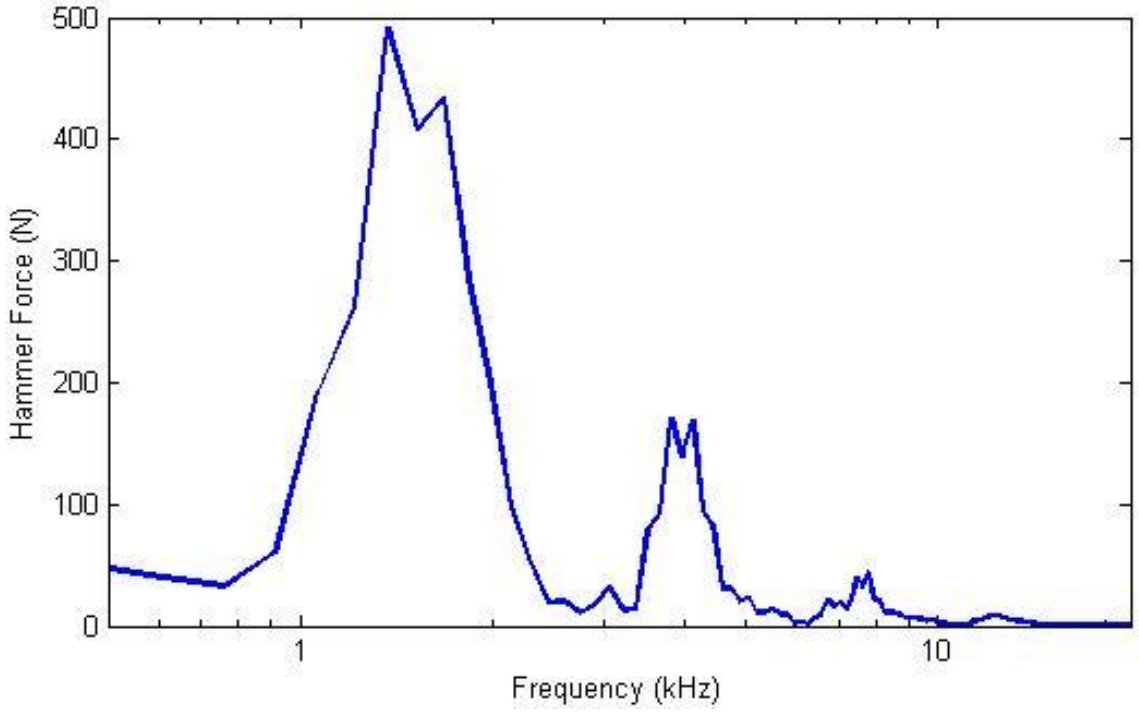

Figure 12: Frequency content of hammer strike over 150 Hz bands

Figure 13 plots the pressure for hydrophone 2 for the model pile. Zooming in on the first few milliseconds of pressure data and plotting it with the force waveform yields some insights. This is shown in Figure 14. The primary frequency in the first 9 milliseconds of pressure data can be calculated from the dominant period of T = 0.4 ms. This period corresponds to a dominant frequency of 2500 Hz. In addition, pressure signal growth is most likely due to the hammer bounce, not constructive interference from wall reflections.

The frequency contents of the pressure data measured by the hydrophones are shown in Figure 15. The dominant frequency shown in the frequency spectrum for the pressure data is 2500 Hz, which corresponds to the measured dominant period.

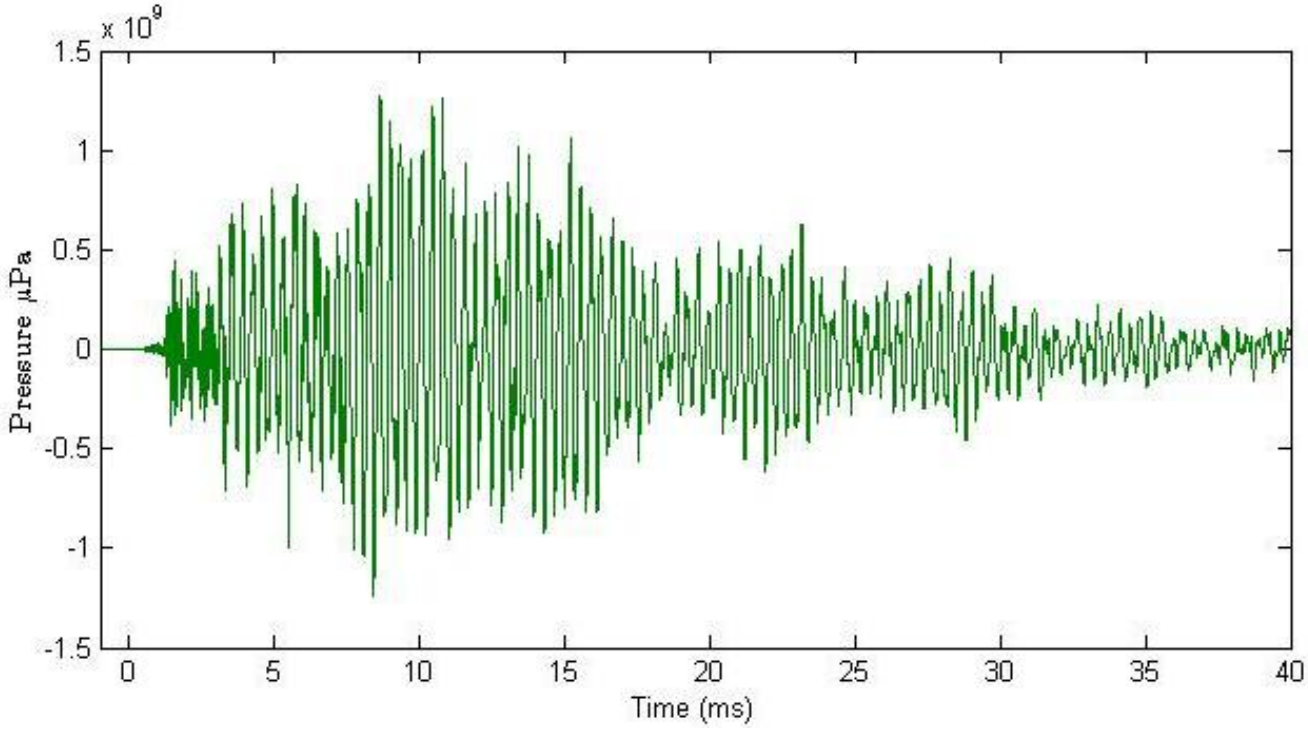

Figure 13: Sound arrival for hydrophone 2 for the model

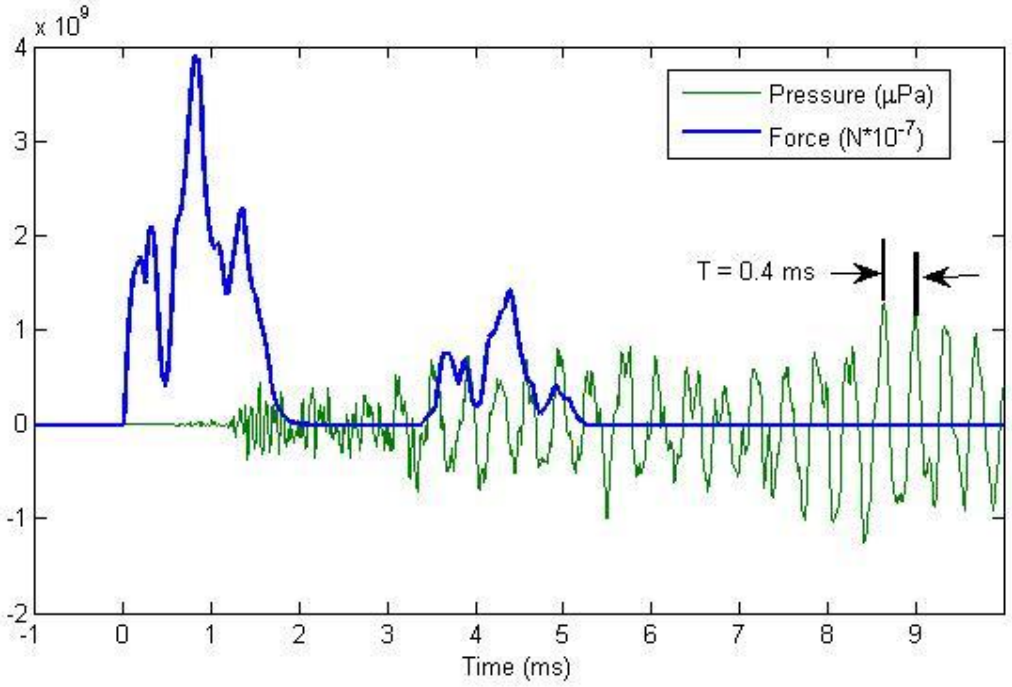

Figure 14: Dominant period measured by hydrophone 2

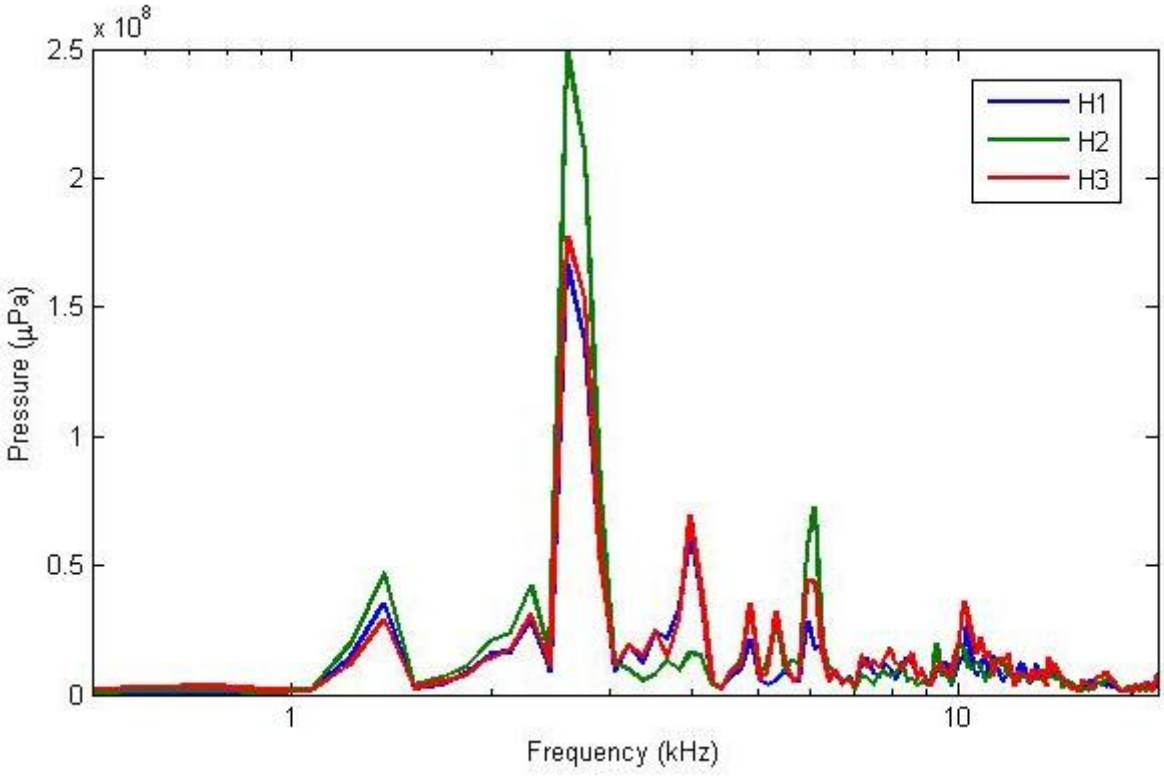

Figure 15: Frequency content measured by the hydrophones over 150 Hz bands

A comparison of the force and pressure data derived from the scaled model with force and pressure data derived from a full-scale CISS pile is shown in Figure 16. The full scale pile has a 0.61 m outer diameter, a length of 27.75 m, and a 0.013 m wall thickness. The full-scale pile is immersed in 4.75 m of air, 7.6 m of water, and 15.5 meters of sediment. The field data are recorded by one hydrophone located at the mid-depth of the water column and 10 m from the pile. Uncertainty in the field data includes the fact that the field data was digitized from a picture of the force and pressure waveforms by manually selecting points from the picture. There are noted similarities in the force waveforms. Both force profiles have a short rise time and a similar shape. The main difference between the field data and the laboratory data is the ratio between force duration and pressure signal duration. Another difference is that more ringing occurs in the laboratory pressure data. This is likely due to the reduced aspect ratio and lack of sediment in the scaled model. To provide more understanding of these differences, future work includes inputting force waveform that is closer to the field force waveform into the model transfer function. The transfer function can be used to find the pressure at a point for any given force waveform. This concept is explored more in the Results section.

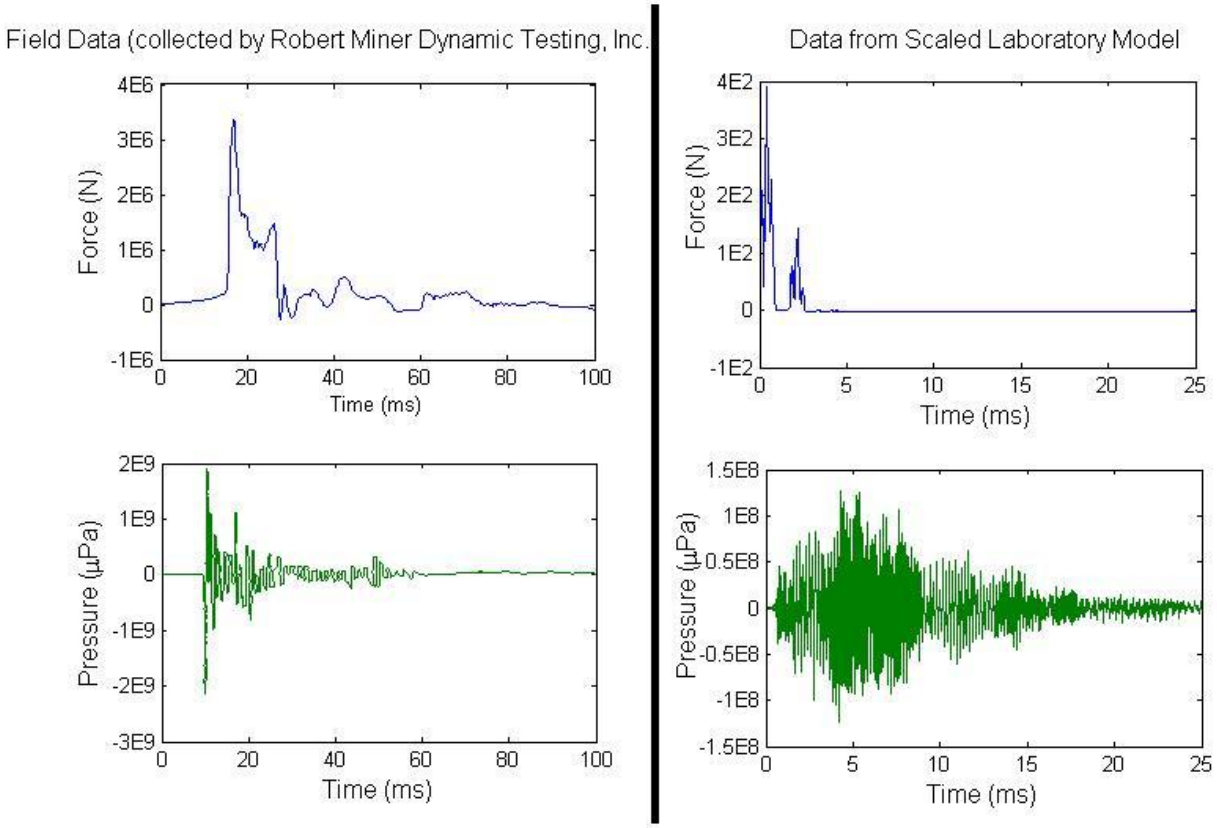

Figure 16: Time-domain comparison between field data and data from scaled model (Robert Miner, 2011)

Sound Exposure

Sound Exposure (*SE*) is used to calculate the root-mean-square pressure (p_{rms}) of a transient pressure waveform. The equation for *SE* is shown below:

$$SE = \int_{t_0}^{t} p^2 dt \tag{11}$$

SE is plotted against time in Figure 17 for the direct sound arrival for hydrophone 2 for the model pile. The time it takes for *SE* to go from 5% to 95% of its final value is 24 ms.

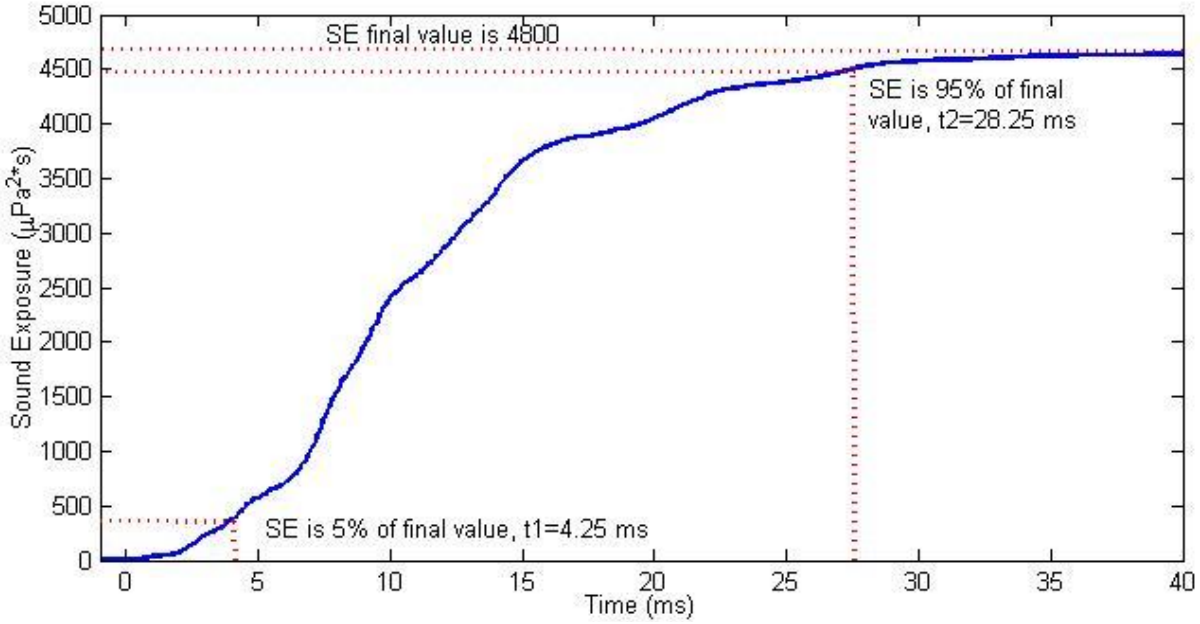

Figure 17: Sound exposure for hydrophone 2

The value for p_{rms} is determined by the following equation, using the t_1 and t_2 found in Figure 17.

$$p_{rms} = \sqrt{\frac{1}{t_2 - t_1}\int_{t_1}^{t_2}[p(t)]^2 dt} \quad \textbf{(12)}$$

The integration to find p_{rms} is performed discretely. The calculated value for p_{rms} for hydrophone 2 is 41.9 x 10^6 μPa. Figure 18 shows the portion of the pressure that is integrated to find SE.

Sound exposure level (SEL) is defined in Equation (13):

$$SEL = 10\log(SE) \quad \textbf{(13)}$$

SEL for the full-size pile and the model pile are shown in Figures 19 and 20, respectively.

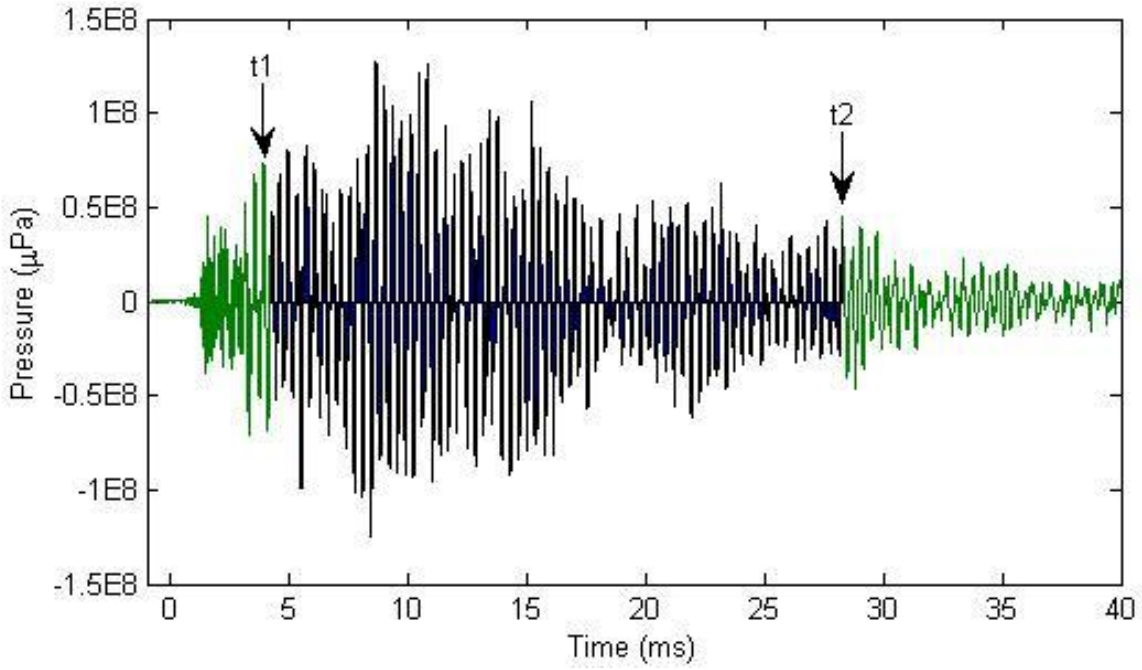

Figure 18: Portion of the pressure waveform that is integrated to find SE

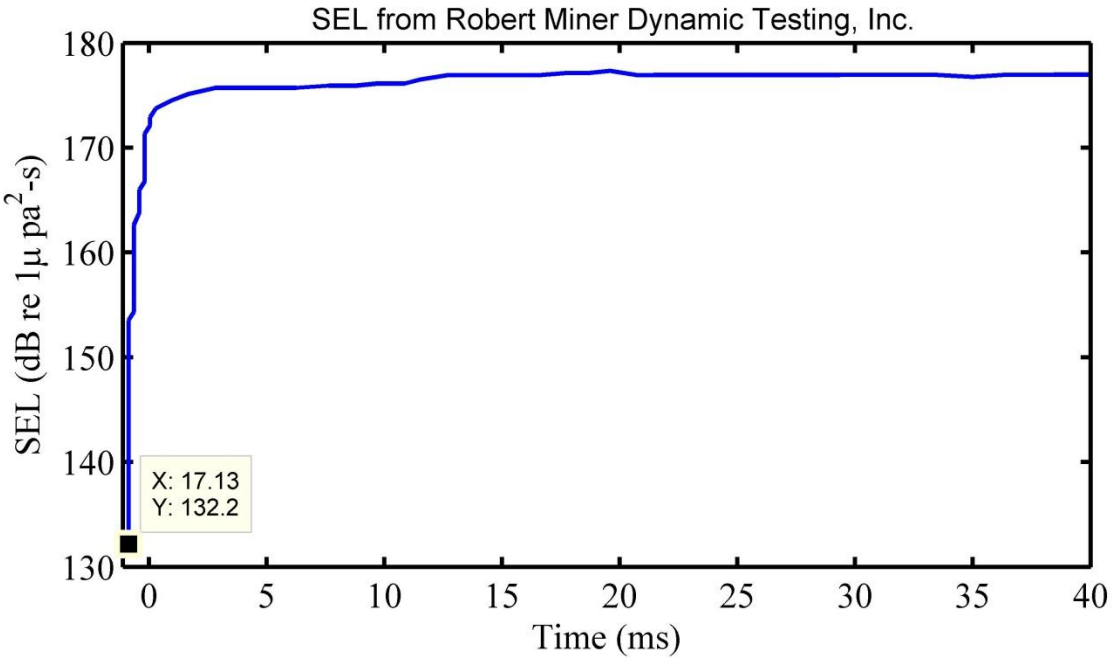

Figure 19: SEL for the field pile

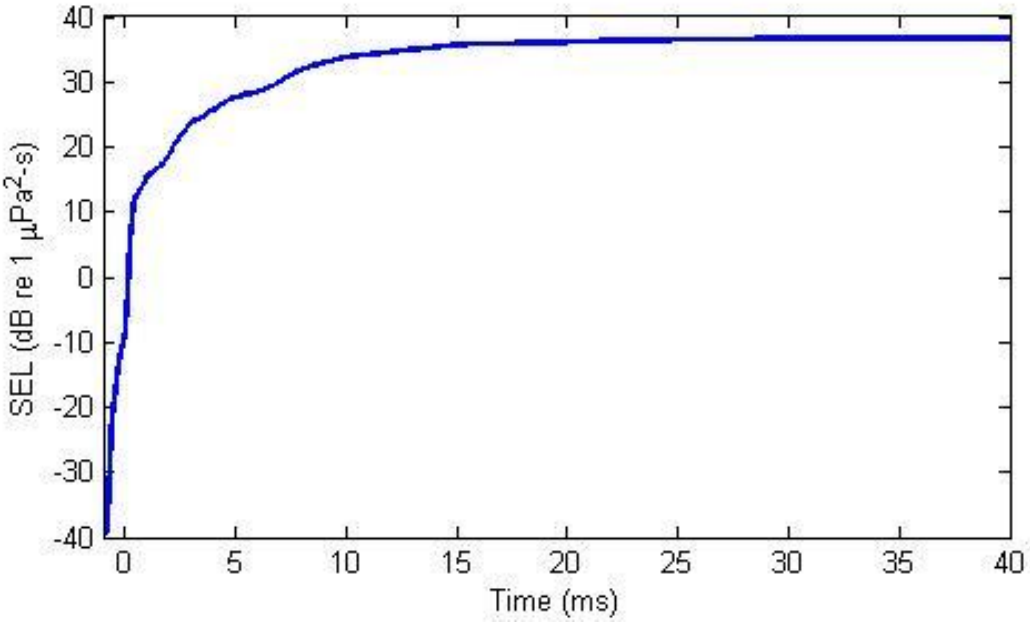

Figure 20: SEL for model pile

Wall Motion

The time domain data collected from accelerometer 2 are shown in Figure 21. It is important to note that the radial wall motion captured by the accelerometer extends much longer in time than the duration of the hammer signal. There is a null in the acceleration data that corresponds to a time of approximately 3 ms. After this null, the waveform increases in amplitude due to the hammer bounce. A zoomed-in comparison of the wall acceleration with the force is shown in Figure 22. The hammer bounce influences the acceleration by increasing the amplitude of vibration after 5 ms.

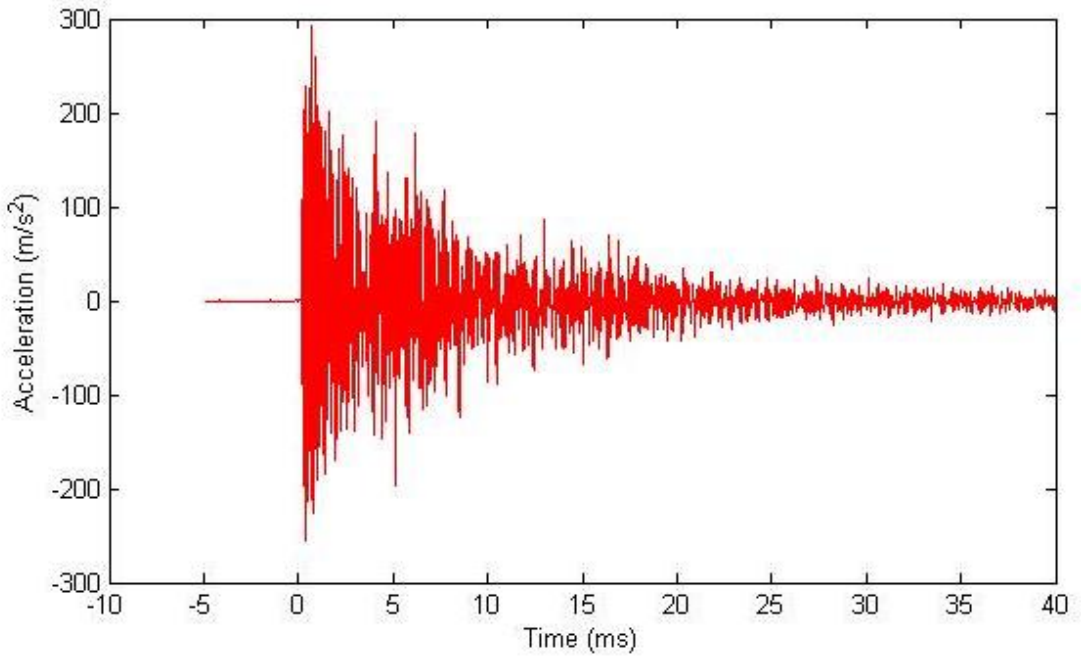

Figure 21: Radial pile wall acceleration given by accelerometer 2

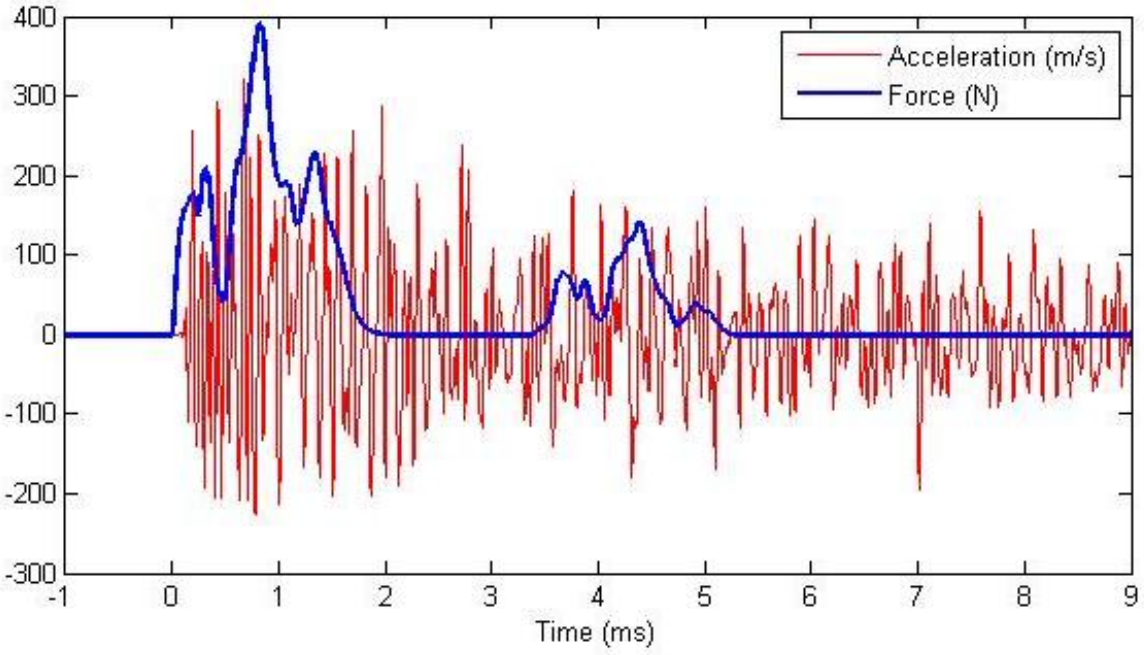

Figure 22: Zoomed- in comparison between force waveform and acceleration waveform

The data collected by the laser are shown in Figure 23. This data represents the radial wall velocity of the pile underwater at a point 0.3 m from the bottom of the model pile. The laser data was subject to very low-frequency interference because of difficulty in isolating the laser vibrometer from the floor. Therefore, the laser data is filtered by a high-pass 4^{th} order Butterworth filter with a cutoff frequency of 100 Hz.

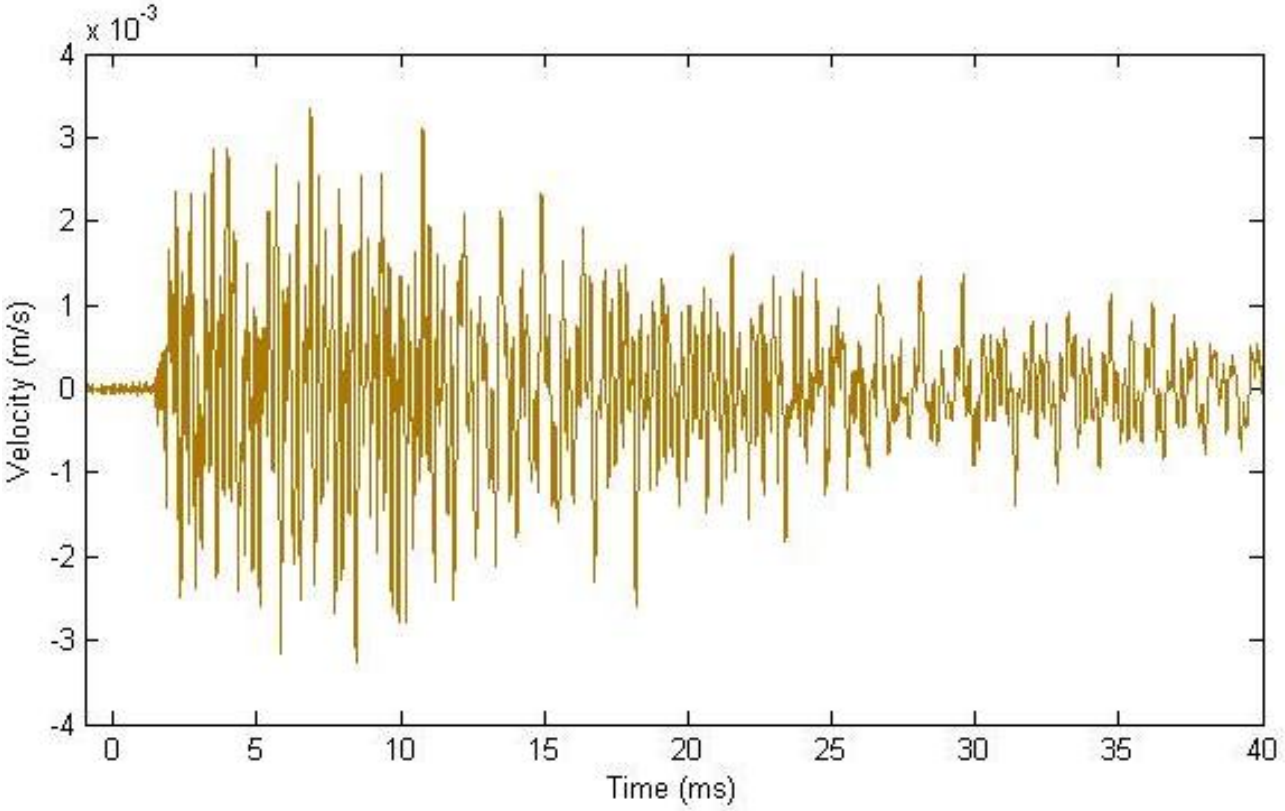

Figure 23: Underwater radial wall velocity of pile as measured by PDV laser

The frequency contents of the center accelerometer and the laser are shown in the following figure. It is important to compare this data to the frequency content measured by the laser to understand the effects of the water upon the vibration of the partially submerged model pile in the radial direction. The accelerometer measures the radial wall motion of the outside surface of the model in air, and the laser measures the radial wall motion on the outside surface in the

submerged portion of the pile. Because the laser measures wall velocity and the accelerometer measures acceleration, the discrete accelerometer data is integrated in the frequency domain by dividing by the angular frequency, ω. The figure shows a large drop in radial wall velocity in the submerged portion of the model. This is due to the loading effect of the water. The frequency range of the laser is 0.5 Hz to 22 kHz. It is impossible to draw experimental conclusions about the effects of water loading at frequencies above 22 kHz. In addition, the cutoff between the mid frequency range and the high frequency range was previously calculated to be 21 kHz for this model pile. In accordance with these restrictions, no frequencies above 20 kHz are plotted for any spectrum plots.

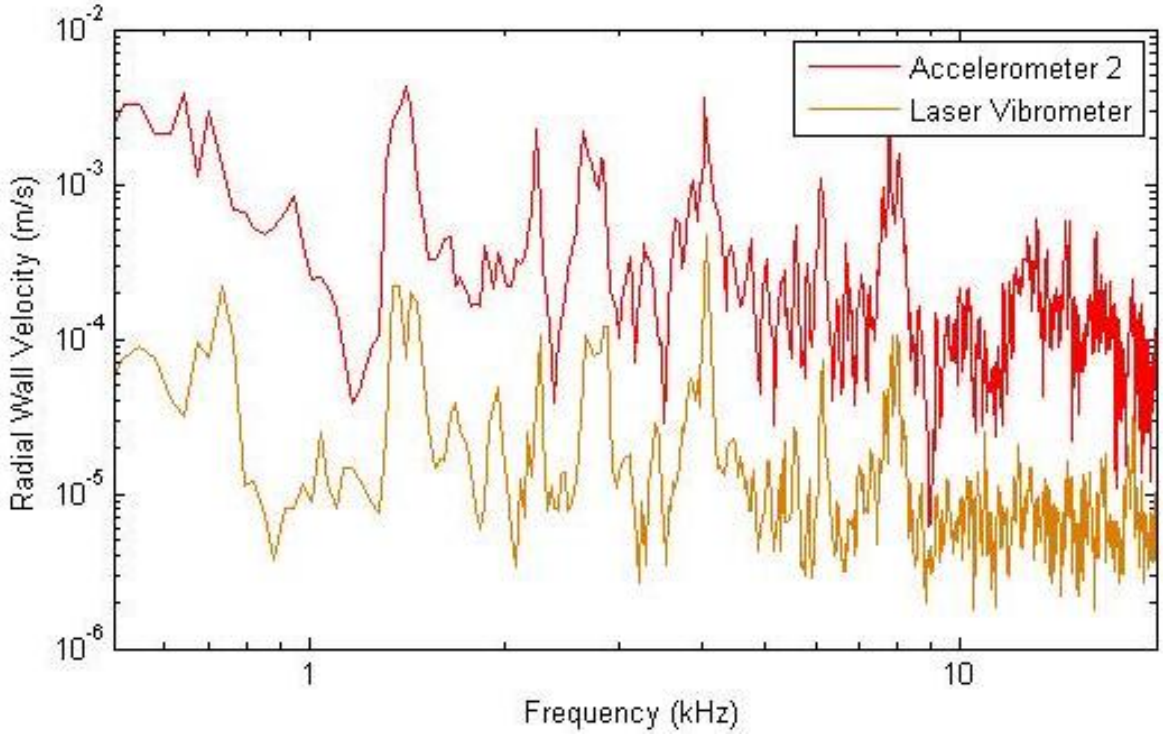

Figure 24: The effects of fluid loading on the radial wall motion over 150 Hz bands

Acoustic Particle Velocity

Particle velocity is not a parameter that has been measured in field data. Nevertheless, particle velocity is an important parameter to measure because it provides more understanding of the sound field. Another reason to measure particle velocity is because fish have been shown to respond to particle velocity, and the ability to predict particle velocity for a full scale pile would help to determine the effects of pile construction on local wildlife (Hastings and Popper, 2005).

Pressure data was collected at nine measurement locations, shown below. Each hydrophone (1 through 4) measures pressure in a cube with these coordinates, allowing particle velocity vectors to be calculated for each hydrophone. Because the measurement cube is only 1 cm^2, the direction vectors are in cylindrical coordinates rather than Cartesian coordinates.

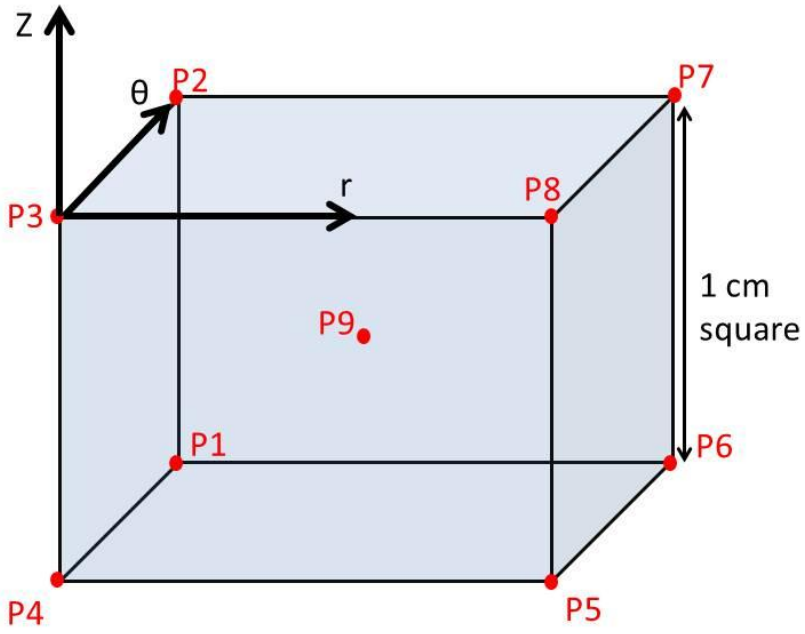

Figure 25: Hydrophone measurement positions and direction vectors

Pressure gradients in the cylindrical coordinates are shown in equations 14, 15, and 16. This gives the right-hand side of Euler's equation. All these calculations are done in the time domain.

$$\Delta p_z = [p_2 + p_3 + p_7 + p_8] - [p_1 + p_6 + p_5 + p_4] \quad \textbf{(14)}$$

$$\Delta p_r = [p_8 + p_7 + p_6 + p_5] - [p_4 + p_3 + p_2 + p_1] \quad \textbf{(15)}$$

$$\Delta p_\theta = [p_2 + p_6 + p_7 + p_1] - [p_3 + p_8 + p_5 + p_4] \quad \textbf{(16)}$$

Figure 26 shows the results of the pressure gradient calculations. Euler's Equation (9) is applied here discretely. The negative of each pressure gradient is integrated with respect to time and divided by the ambient density of fresh water at 17 °C, 998 kg/m^3. This results in the particle velocity vectors in cylindrical coordinates, plotted in Figure 27.

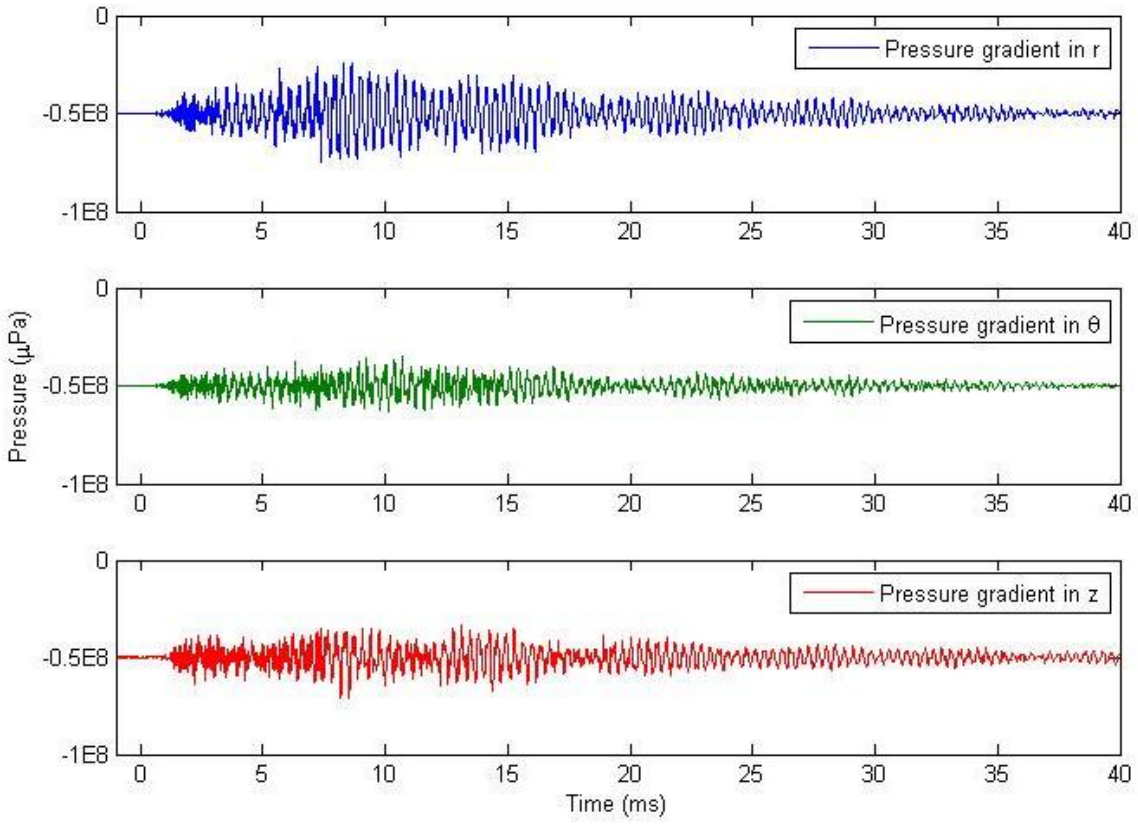

Figure 26: Pressure gradients for hydrophone 2 in the r, θ, and z directions. Note that the pressure gradient in r is the largest.

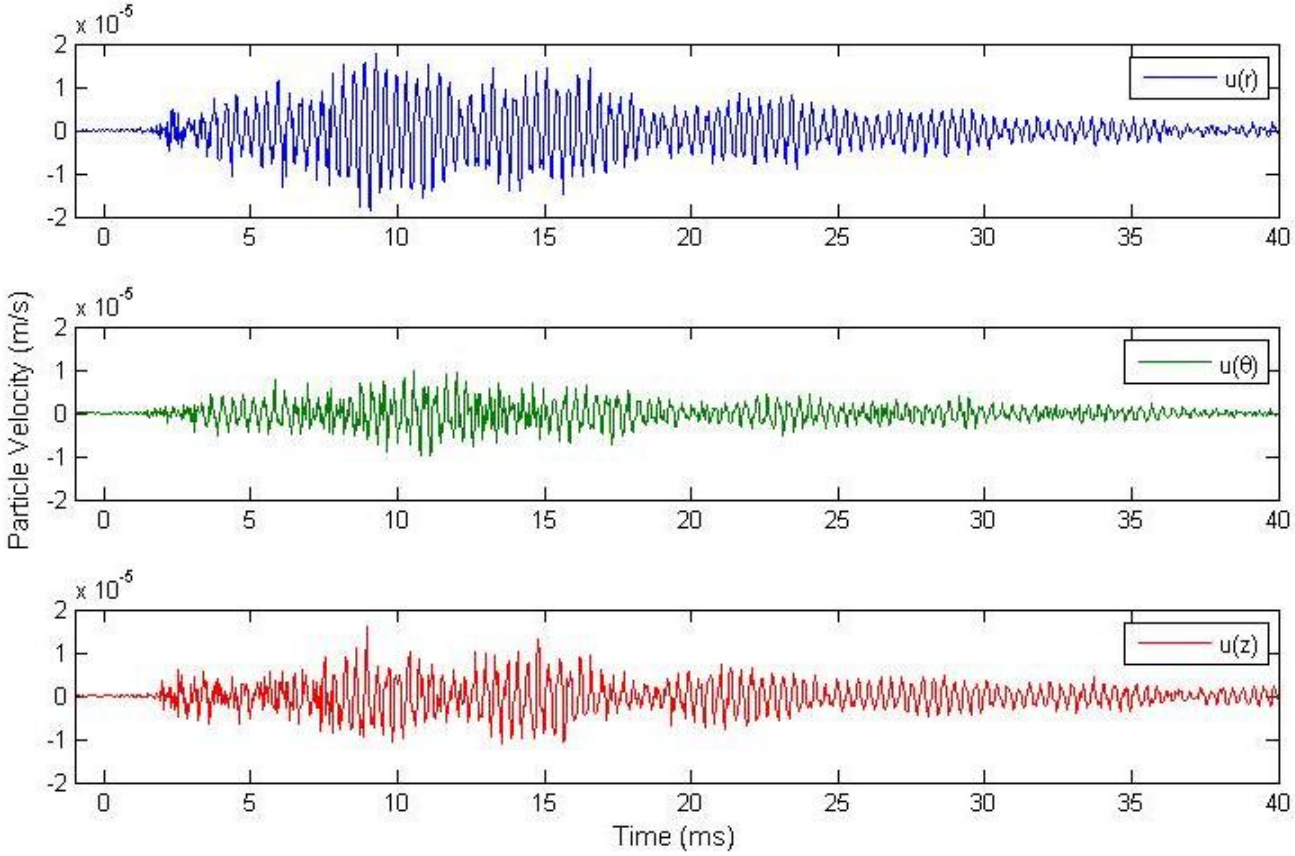

Figure 27: Particle velocity vectors for hydrophone 2

Cross Correlation between Radial Wall Acceleration and Pressure

Because the pressure signal dispersion distorts the signal, it is necessary to use the method of cross correlation to statistically determine the time lag between the radial wall acceleration measured at accelerometer 2 and the pressure measured by hydrophone 2. This correlation is normalized so that the maximum correlation has a value of 1. The time lag for the maximum correlation is 0.27 ms. The normalized correlation is plotted as a function of time lags in Figure 28.

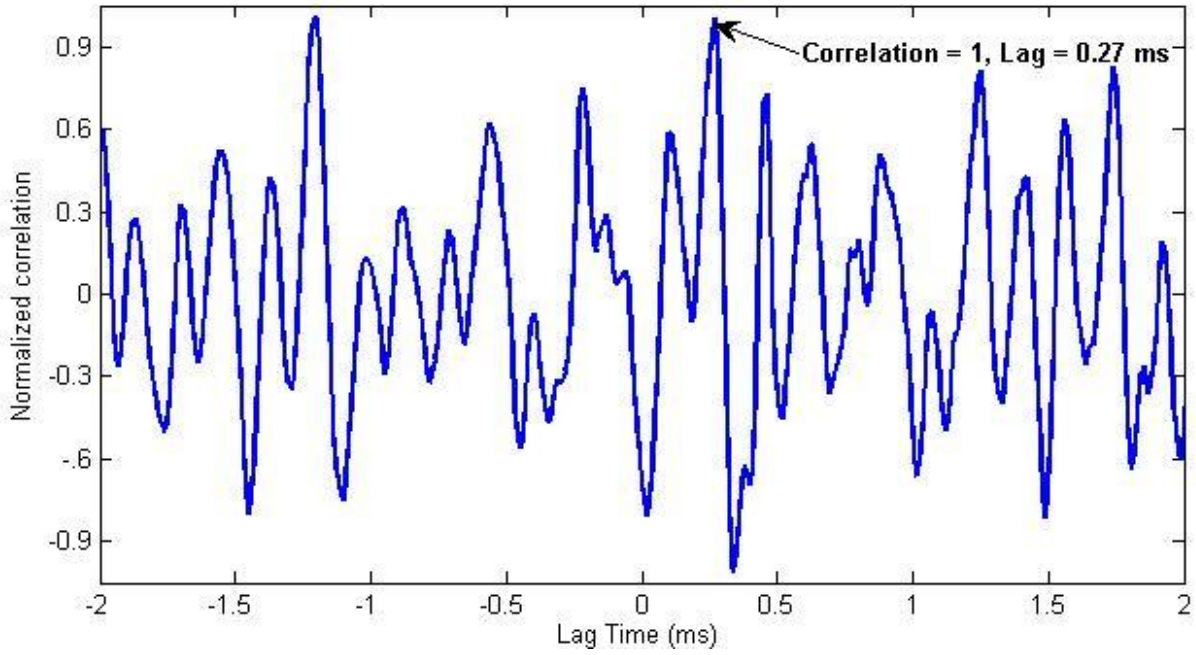

Figure 28: Cross correlation between radial wall acceleration at A2 and pressure at H2

Results

Instantaneous Intensity

Instantaneous acoustic intensity in the r, θ, and z directions is calculated by multiplying instantaneous pressure with the instantaneous particle velocity. Particle velocity was calculated previously. The pressure that multiplies the particle velocity to get intensity is the average of all nine measurement locations. Figure 29 shows that the absolute value of the intensity in the radial direction is much greater than the intensities in the longitudinal and circumferential directions. In addition, the radial intensity is largely negative (i.e. the intensity vector is pointed towards the model pile). The intensity in the z (or longitudinal) direction is influenced by the boundary effects of the air/water interface. Yet even with these boundary effects, the intensity is still largest in the radial direction. This result is not surprising because pile particle velocity in the radial direction is tangent to the fluid/steel interface, maximizing radiation coupling in this direction. Intensity values during and immediately after the hammer strike will be examined further in the energy analysis section.

It is necessary to compare the instantaneous radial intensities for hydrophones 1, 2, and 3. This provides an understanding of how the radiated field changes with depth. Figure 30 plots the radial component of acoustic intensity for each of the three hydrophone locations. Hydrophone 2, located at the mid-depth of the water, shows the largest absolute value of intensity.

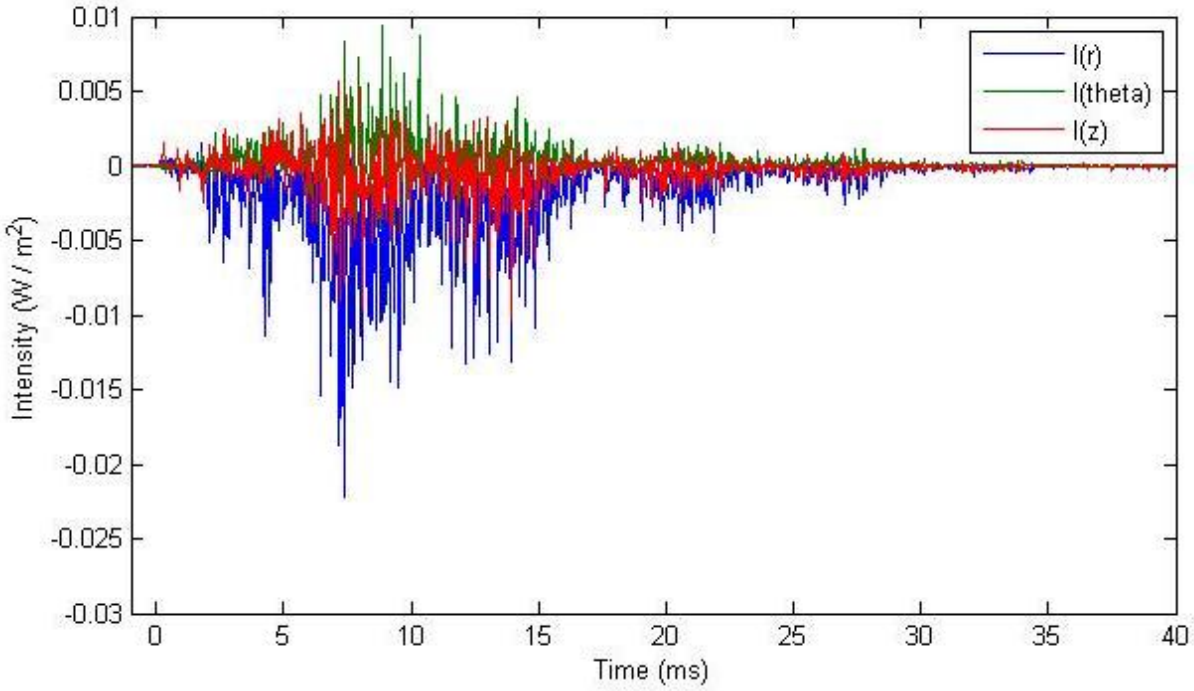

Figure 29: Instantaneous intensity vector components for hydrophone 2

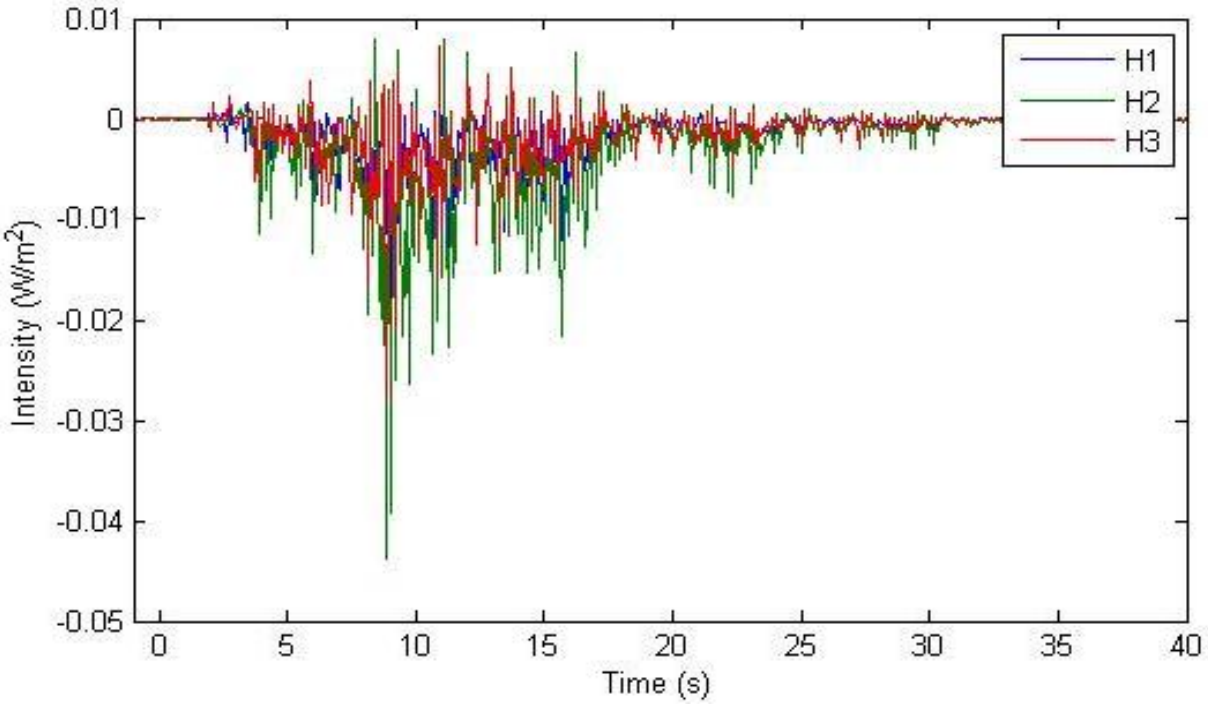

Figure 30: Instantaneous acoustic intensity for the three hydrophone positions

Transfer function between applied force and sound pressure at a point

To be able to find the pressure at a point for any given input force, it is necessary to determine the transfer functions between the applied force and pressures measured by hydrophones 1, 2, and 3. The transfer function was found from the quotient of the cross power spectral density the force and pressure data and the power spectral density of the force data. The data was zero-padded to the next power of two before performing the FFT. A periodic hamming window was applied with length equal to the signal segment length that results from dividing the force signal into eight sections and then applying 50% overlap. This gives the impulse response spectra for the pressure at the indicated hydrophone positions. Figure 31 illustrates the effects of the system upon the input force. This function is only plotted for frequencies from 0.5 kHz to 7 kHz because the hammer does not apply a force to the model pile above 7 kHz. Frequencies of 2700 Hz and 5900 Hz are amplified by the system. When this transfer function is compared to the pressure frequency spectrum, it is easy to see that other frequencies which appear to be resonances, such as 1500 Hz and 4000 Hz, are actually dominant frequencies from the force spectrum that are being transmitted to the pressure spectrum.

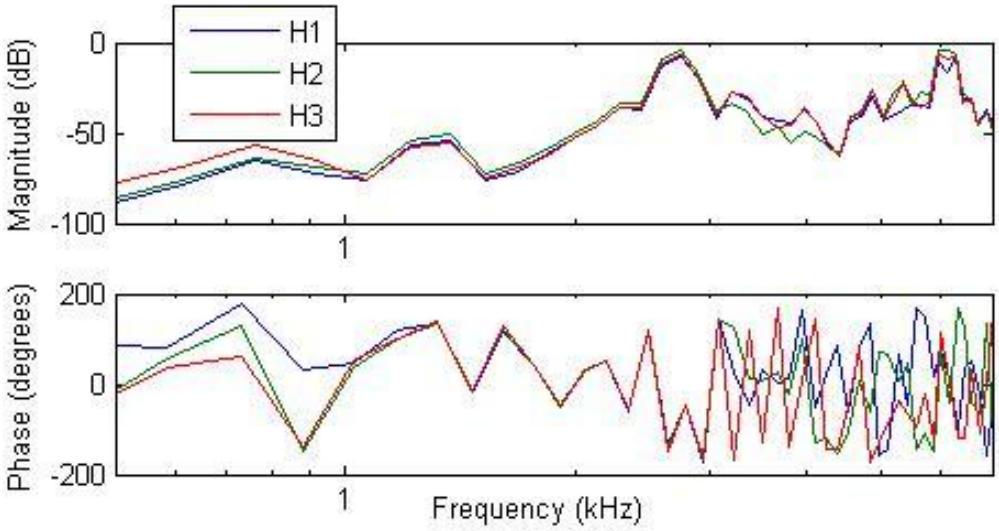

Figure 31: Transfer function between applied force and sound pressure over 150 Hz bands (0dB corresponds to 3.39 x 10^7 µPa/N)

Energy Exchange at the Measurement Surface

Because of the axisymmetric properties of the scale model, the intensity measurements conducted by hydrophones 1, 2, and 3, as well as the wall surface acceleration measurements, can be used to determine the total energy change in the volume enclosed by the measurement surface defined in Figure 32. The top surface of the measurement surface cylinder is not counted in the calculations because the energy loss through the top of the cylinder is deemed to be negligible compared to the energy emitted in the radial direction.

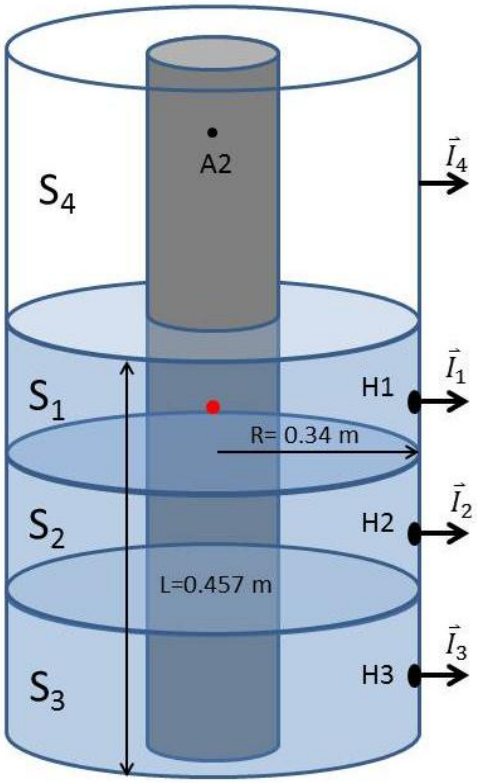

Figure 32: Measurement surfaces and intensity vectors for energy analysis (figure not to scale)

The integral to find the total change in energy of the volume throughout time is conducted discretely. The surface *S* is divided into four areas: S_1, S_2, S_3, and S_4.The underwater portion of the volume is divided into three equal parts. Therefore, $S_1 = S_2 = S_3 = 0.325$ m^2 and $S_4 = 0.976$ m^2.

As stated before, the total model pile length is 0.914 m. The blue in the figure is the volume that contains water. The volume contained by S_4 is in air. All intensity vectors are in the radial direction, perpendicular to the surfaces. The discrete approximation to the spatial integral is shown below:

$$\iint_S \; I_n \, dS = \vec{I}_1 S_1 + \vec{I}_2 S_2 + \vec{I}_3 S_3 + \vec{I}_4 S_4 \qquad \textbf{(17)}$$

While the intensities underwater calculated from pressure gradients measured by hydrophones 1, 2, and 3, the intensity at R=0.34 m in air must be calculated from the measured wall acceleration at accelerometer 2. To approximate I_4 in the radial direction, we must make the approximation of plane waves in air. This is a valid approximation for most of the frequency range of interest because most wavelengths in air in the frequency range of 3 kHz to 20 kHz are several orders of magnitude smaller than the diameter of the pile model. Therefore, with the plane wave assumption:

$$\overrightarrow{I_4} = \rho_0 c U^2 \qquad \textbf{(18)}$$

where $\rho_0 c$ is the characteristic impedance of air and U is the wall velocity. The measured acceleration is integrated to find the wall velocity. Because the intensity in air is several orders of magnitude higher than the intensity in water, the energy integrals in air and water are calculated separately so that the phenomena in the water can be looked at separately instead of being dominated by the phenomena in air. The instantaneous acoustic power at the boundary in water is shown in Figure 33. The positive acoustic power at the boundary in water means that energy is being added to the shell by the water. This corresponds to the negative radial intensity discussed in previously. However, the largely positive portion of the acoustic power occurs after 2 ms, which signals the end of the hammer strike. Until 2 ms, energy is transported to the water

from the shell. Because the air imports negligible loading on the shell, there is negligible energy transmitted from the air to the shell.

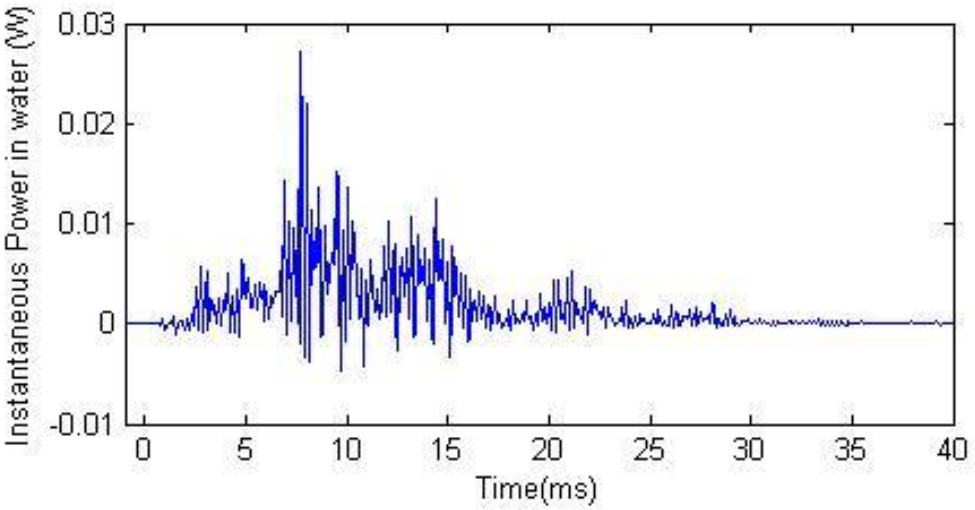

Figure 33: Instantaneous acoustic power calculated at the shell surface in water. Positive power implies that energy is being added into the control volume

Figure 34 shows a zoomed-in version of Figure 33. Figure 34 illustrates the drastic increase in power added to the shell after the end of the first hammer bounce.

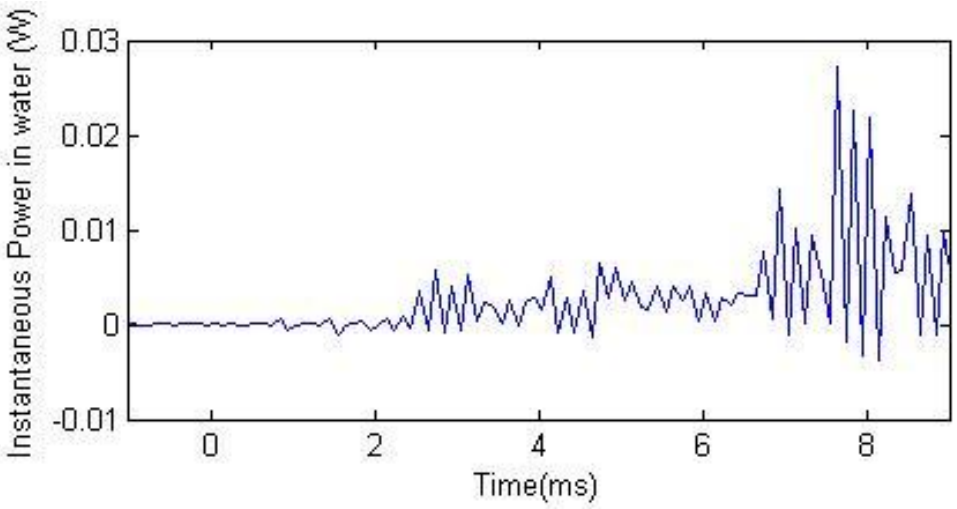

Figure 34: Zoomed-in view of acoustic power. Note the rise in power transmitted into the shell from the surrounding water after 2 ms.

The time-integrated acoustic powers in water and in air are shown in Figures 35 and 36. This metric is an indication of the cumulative amount of energy radiated from the structure that flows back into the structure from the water.

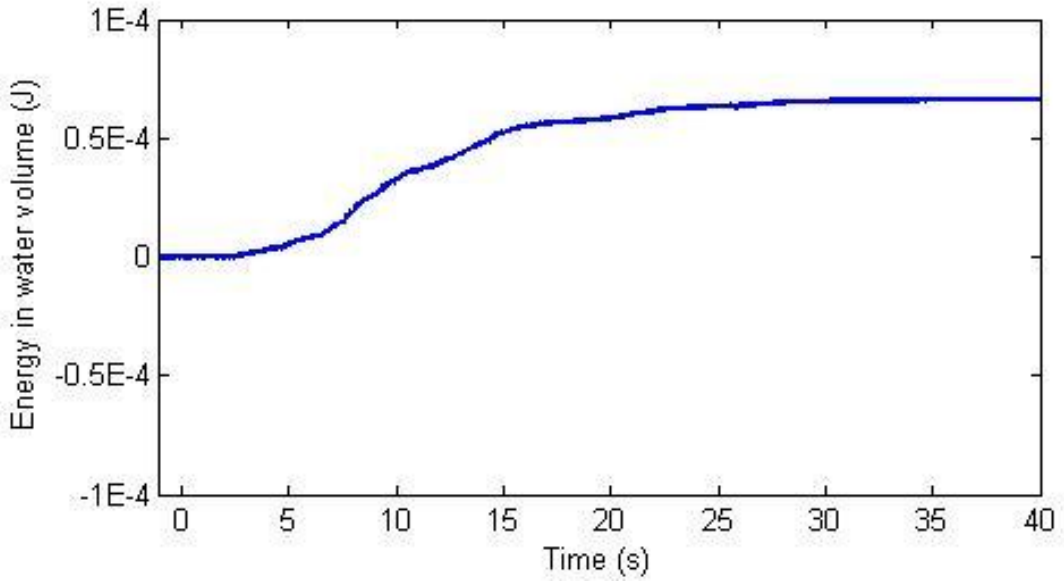

Figure 35: Cumulative acoustic energy passing through the shell surface in water. Positive energy implies that energy is entering the control volume

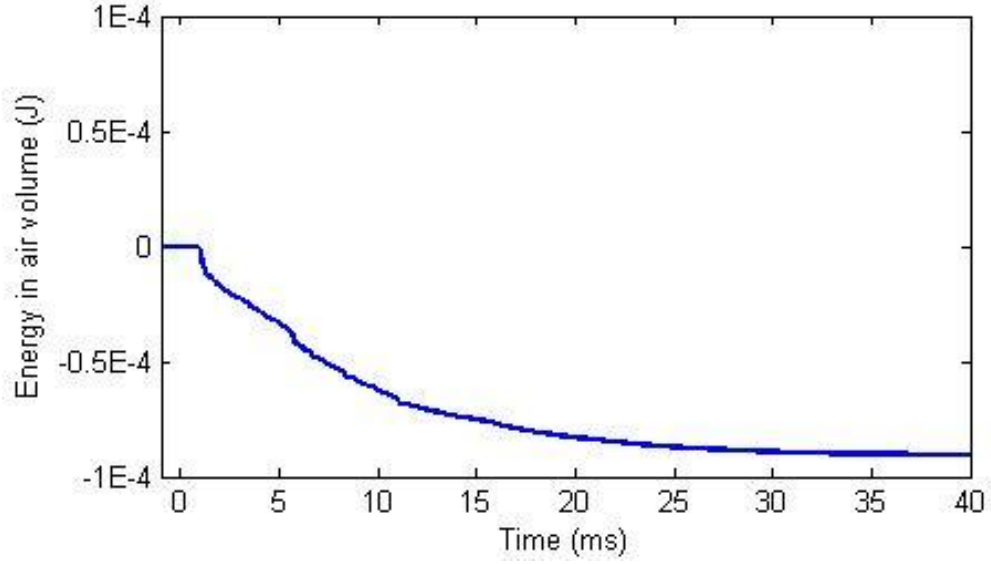

Figure 36: Cumulative acoustic energy passing through the shell surface in air. Negative energy implies that energy is leaving the control volume

Conclusions and Recommendations

This study provides a more detailed understanding of some of the complex interactions between the impact force, steel pile, and water during the generation and propagation of sound.

Time domain analysis of the system is important because the force has finite time duration, and therefore the behavior of the system is transient. In the time domain, the energy exchange between the structure and the acoustic field was analyzed as it occurred. The most interesting observation was that a significant portion of the energy that enters the fluid while the force is active re-enters the structure immediately following the duration of the force. This implies that the highly damped acoustic waveform observed in the field data is a result of energy returning to the pile from the water (ICF Jones & Stokes and Illingworth and Rodkin, 2009). This phenomenon must be included in mathematical models to accurately simulate pile noise. Future work includes using near-field hydrophones to examine this fluid-structure interaction closer to the pile.

The frequency analysis shows how the transfer function spectrum is dominated by a few frequencies. This is likely due to irregularities in the hammer force. The signal processing techniques used in this study are useful means to study the vibration of and acoustic radiation from a cylindrical shell under impact. Specifically, the effects of different force time histories can be determined from the transfer functions. Future work includes investigating the effects of the hammer strike waveform to on the sound radiation, similar to the work done by Mann et al. (1991).

Appendix: Calibration Sheets

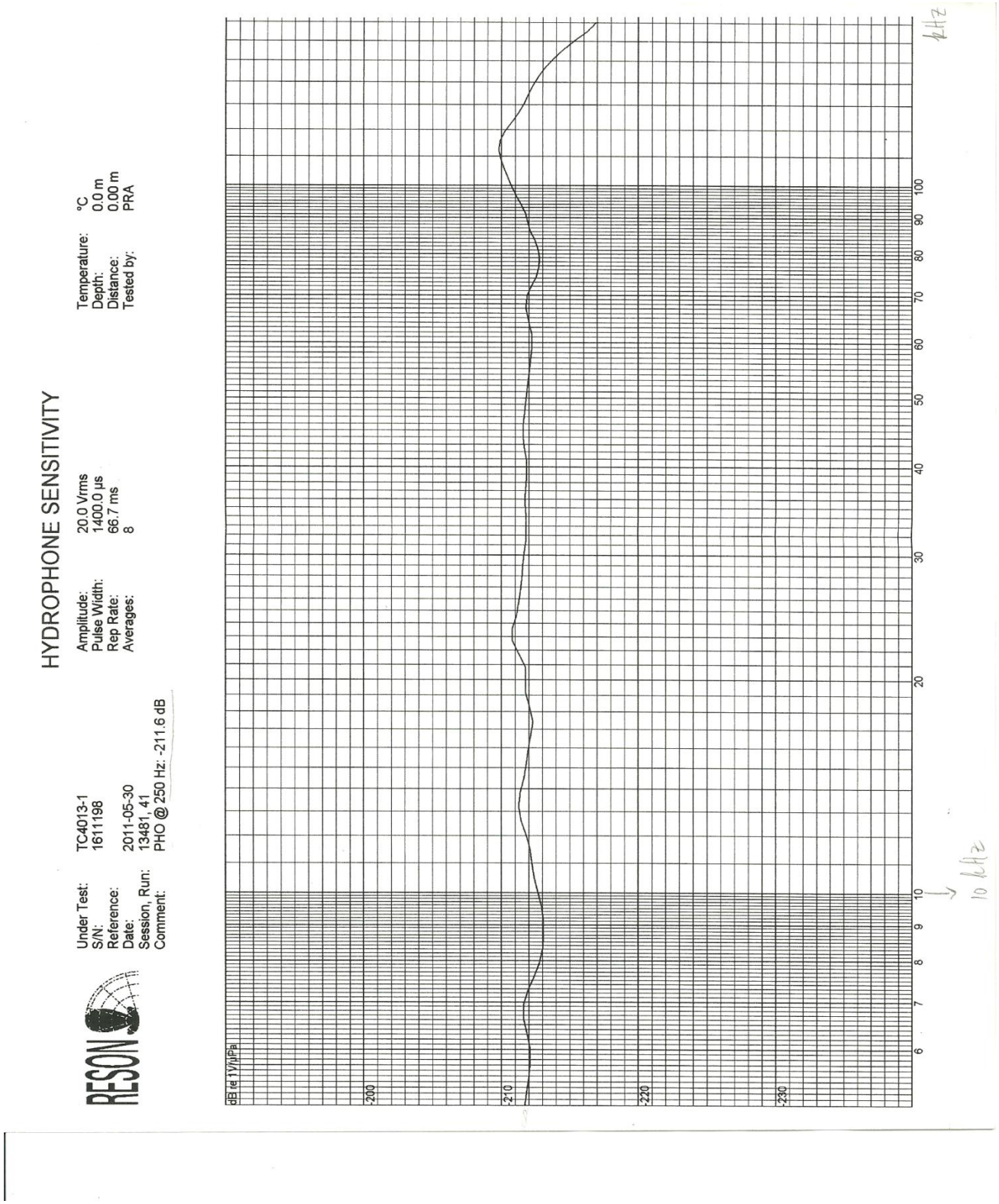

HYDROPHONE SENSITIVITY

RESON

Under Test:	TC4013-1	Amplitude:	20.0 Vrms	Temperature:	°C
S/N:	1611216	Pulse Width:	1400.0 µs	Depth:	0.0 m
Reference:		Rep Rate:	66.7 ms	Distance:	0.00 m
Date:	2011-05-30	Averages:	8	Tested by:	PRA
Session, Run:	13481, 25				
Comment:	PHO @ 250 Hz: -211.5 dB				

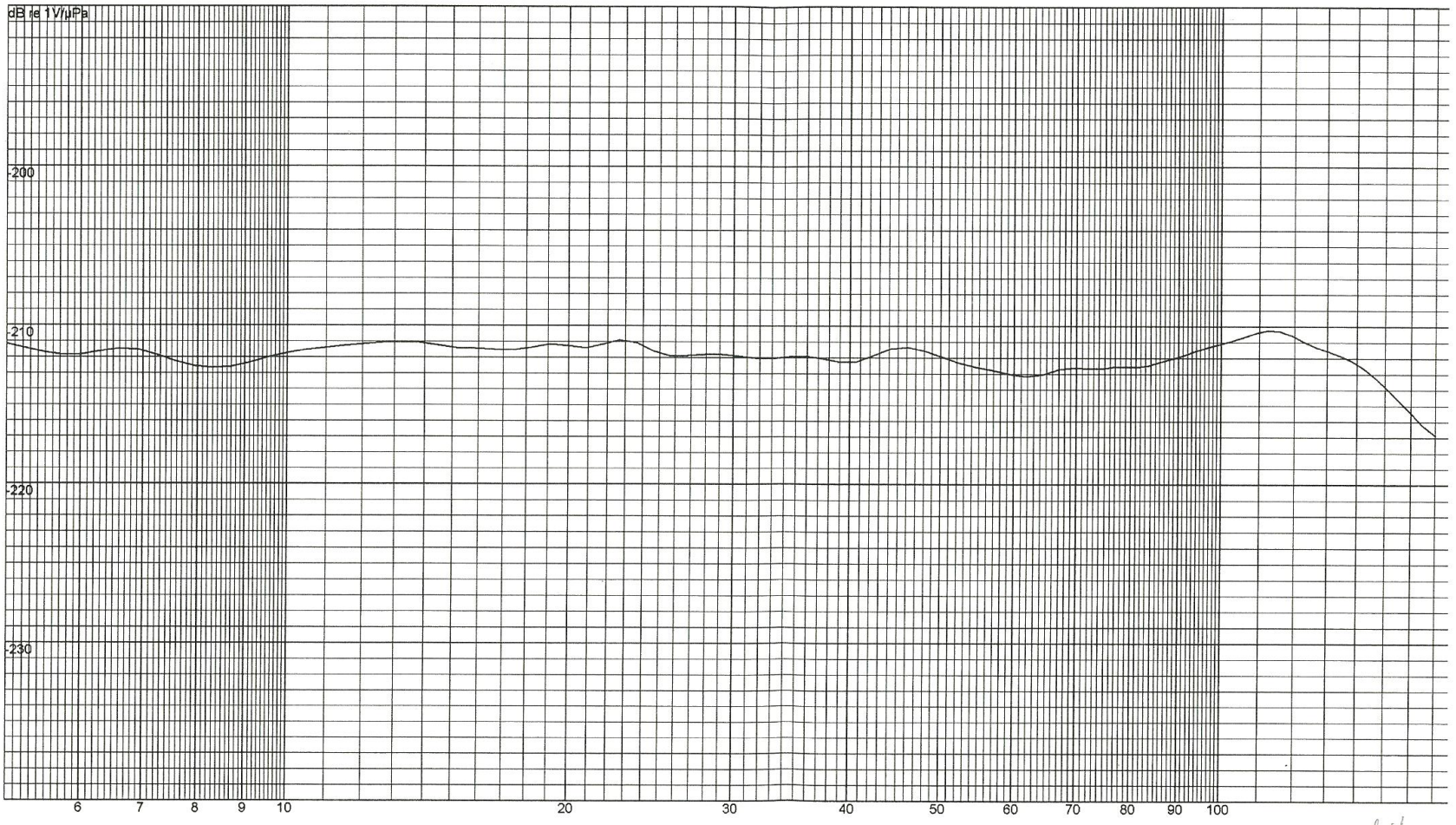

HYDROPHONE SENSITIVITY

RESON

Under Test:	TC4013-1	Amplitude:	20.0 Vrms	Temperature:	°C
S/N:	1611210	Pulse Width:	1400.0 µs	Depth:	0.0 m
Reference:		Rep Rate:	66.7 ms	Distance:	0.00 m
Date:	2011-05-31	Averages:	8	Tested by:	PRA
Session, Run:	13488, 58				
Comment:	PHO @ 250 Hz: -211.7 dB				

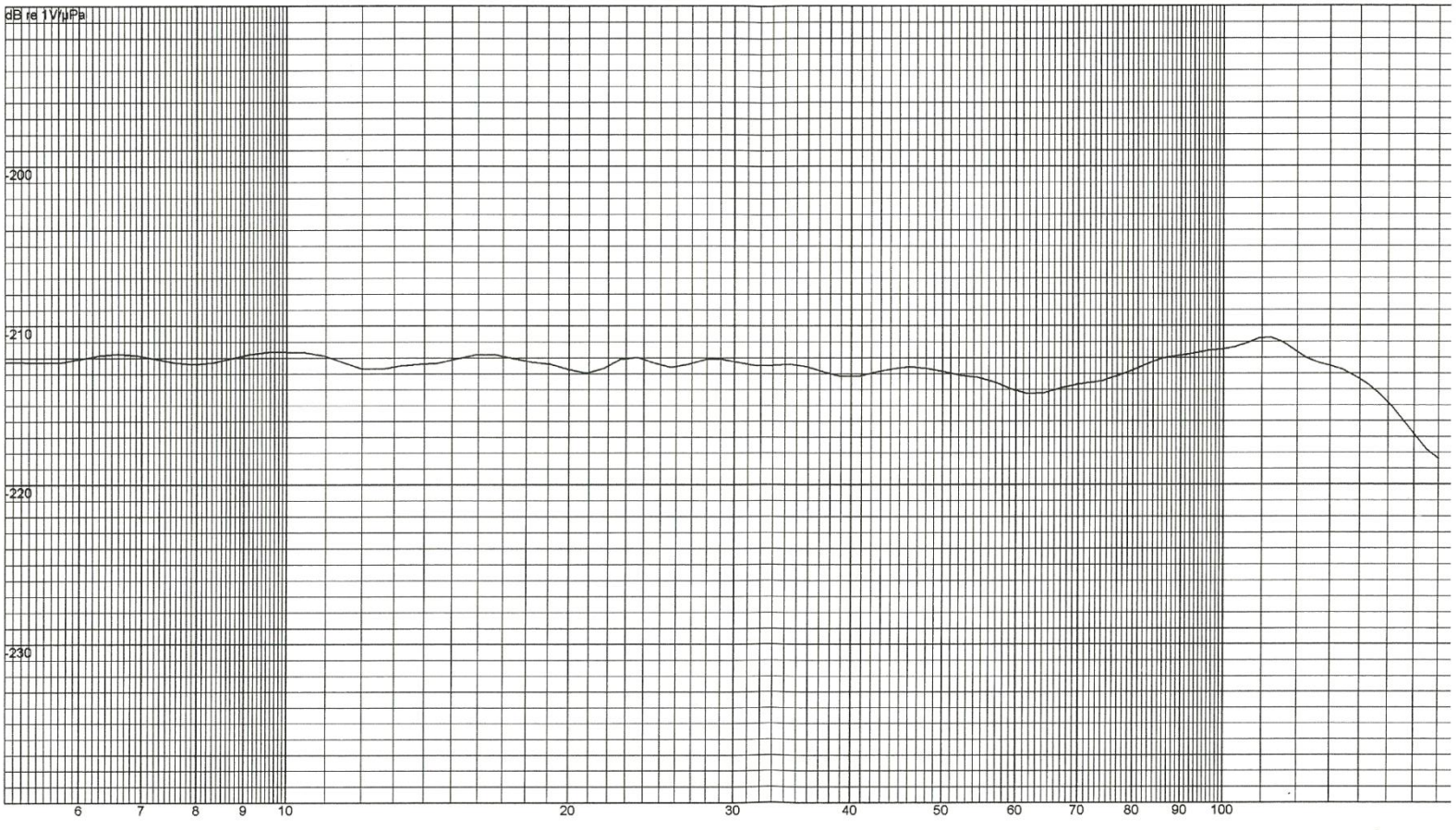

~Calibration Certificate~

Model No.: 086E80 Customer: _____

Serial No.: 30076 _____

Description: Impulse Force Hammer PO No.: _____

Manufacturer: PCB Calibration Method: Impulse (AT-303-1)

Data

Output Bias: **9.9** Temperature: 72 °F 22 °C Relative Humidity: 47 %

HAMMER SENSITIVITY:

Hammer Configuration / Tip		Steel	Vinyl	Vinyl
Hammer Configuration / Extender		None	Steel	None
Hammer Sensitivity	mV/lb	104.2	84.47	80.44
	(mV/N)	23.42	18.99	18.09

Above data is valid for all supplied tips.

Condition of Unit:

As Found N/A.

As Left New unit in tolerance.

Notes:

1. Calibration is NIST Traceable thru Project 681/280472 and PTB Traceable thru Project 10065.
2. This certificate may not be reproduced, except in full, without written approval from PCB Piezotronics, Inc..
3. Calibration is performed in compliance with ISO 10012-1, ANSI/NCSL Z540-1-1994.
4. See Manufacturer's specification sheet for a detailed listing of performance specifications.
5. Measurement uncertainty (95% confidence level with a coverage factor of 2) is +/-3.8%.

Technician: Bob Myers RM Date: 7/5/2011

ACCREDITED
CALIBRATION CERT # 1862.01

PCB PIEZOTRONICS INC.
3425 Walden Avenue
Depew, N.Y. 14043

TEL: 716-684-0001 FAX: 716-684-0987 www.pcb.com

Calibration Station: 13

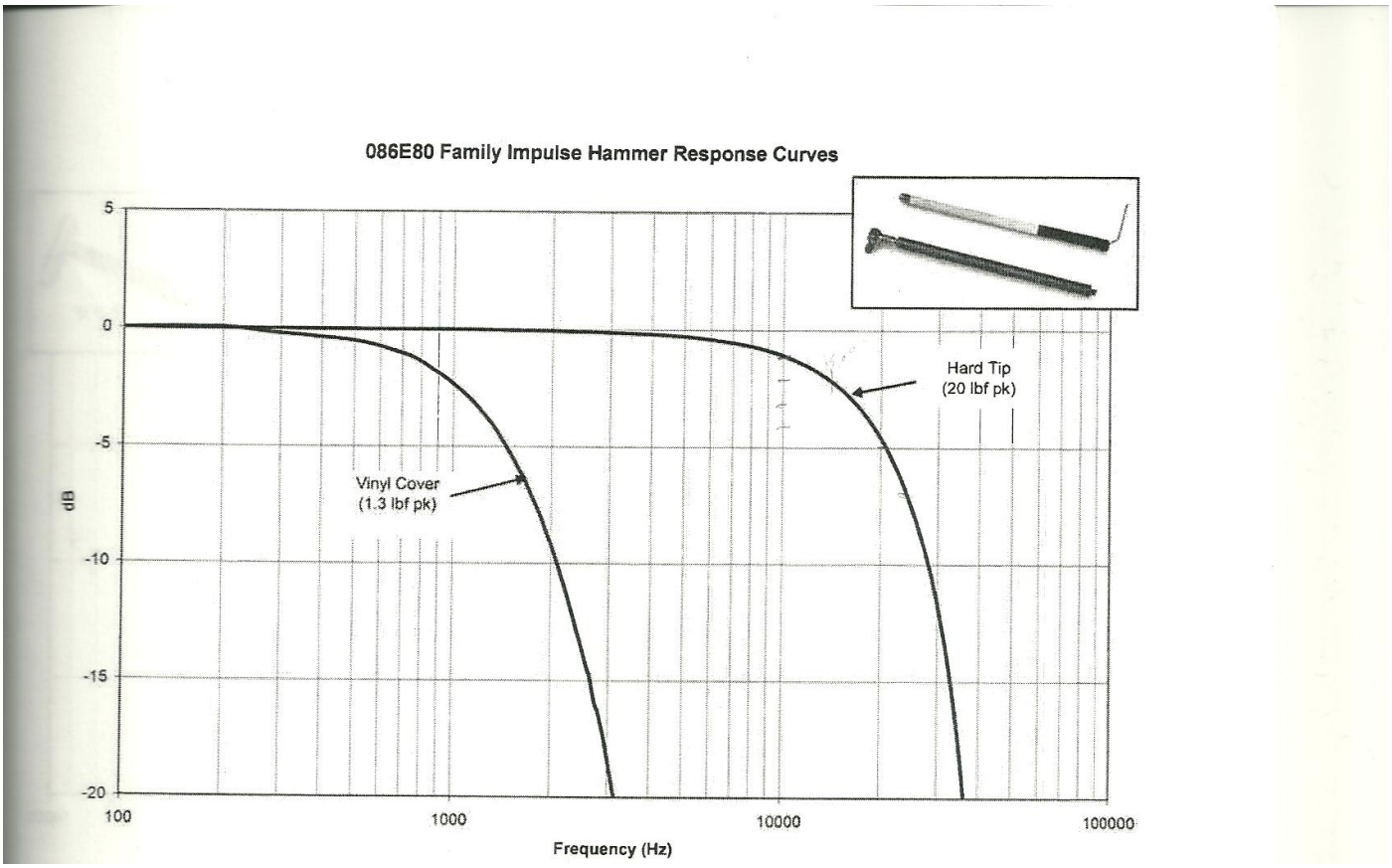
086E80 Family Impulse Hammer Response Curves
5
0
-5
-10
-15
-20
dB
100
1000
10000
100000
Frequency (Hz)
Hard Tip
(20 lbf pk)
Vinyl Cover
(1.3 lbf pk)

圧電式加速度ピックアップ校正表
Calibration Data

型式 Model PV－ 08A 2

製造番号 Serial No. 11855

電荷感度 (80Hz) Charge Sensitivity	0.098	pC/(m/s²)
横感度比 (30Hz) Transverse Sensitivity	3	%
静電容量 Capacitance	423	pF
測定温度 Temperature	22	℃
測定年月 Date	2011.7	

検査責任者 Inspected by 守山

リオン株式会社 RION CO., LTD.

圧電式加速度ピックアップ校正表
Calibration Data

型式 Model PV－ 08A 1

製造番号 Serial No. 11854

電荷感度 (80Hz) Charge Sensitivity	0.098	pC/(m/s²)
横感度比 (30Hz) Transverse Sensitivity	3	%
静電容量 Capacitance	417	pF
測定温度 Temperature	22	℃
測定年月 Date	2011.7	

検査責任者 Inspected by 守山

リオン株式会社 RION CO., LTD.

圧電式加速度ピックアップ校正表
Calibration Data

型式 Model PV－ 08A 3

製造番号 Serial No. 11856

電荷感度 (80Hz) Charge Sensitivity	0.099	pC/(m/s²)
横感度比 (30Hz) Transverse Sensitivity	3	%
静電容量 Capacitance	423	pF
測定温度 Temperature	22	℃
測定年月 Date	2011.7	

検査責任者 Inspected by 守山

リオン株式会社 RION CO., LTD.

References

ASTM D4945 (2008). A standard test method for high-strain dynamic testing of deep foundations, ASTM International.

Burgess, W.C. and Blackwell, S.B. (2005) Underwater acoustic measurements of vibratory pile driving at the Pipeline 5 Crossing in the Snohomish River, Everett, Washington Greeneridge Sciences Report 322-2.

Carlson, T.J. and Weiland, M.A. (2007) Dynamic pile driving and pile driving underwater impulsive sound, technical report to Washington Department of Transportation, http://www.wsdot.wa.gov/research/reports/fullreports/673.1.pdf (accessed June 7, 2012)

De Rosa, S., Franco, F., Li, X. and Polito, T. (2012). A similitude for structural acoustic enclosures, *Elsevier: Mechanical Systems and Signal Processing*, **30:** 330-342.

Gonçalves, P.B. and Batista, R.C. (1986). Frequency response of cylindrical shells partially submerged or filled with fluid, *Journal of Sound and Vibration*, **113:** 59-70.

Hastings, M. and Popper, A. (2005). Effects of sound on fish, Report for the California Department of Transportation.

Hastings, M. (2007). Prediction of underwater noise from large cylindrical piles being driven by impact hammers, Noise-Con, Reno.

Hastings, M. and Shahab, S.(2012). Acoustic source modeling of a partially submerged steel pile, Report for the Oregon Department of Transportation .

ICF Jones & Stokes and Illingworth and Rodkin, Inc. (2009). Technical guidance for assessment and mitigation of the hydroacoustic effects of pile driving on fish, Appendix I, California

Department of Transportation, 2009. http://www.dot.ca.gov/hq/env/bio/files/Guidance_Manual_2_09.pdf (accessed June 12, 2012).

Junger, M.and Feit, D. (1993a). *Sound, Structures, and Their Interactions*, Acoustical Society of America, 195-231.

Junger, M. and Feit, D. (1993b). *Sound, Structures, and Their Interactions*, Acoustical Society of America, 279-309.

Lengua, G.A. (1998). Modeling of membrane waves, Space and Naval Warfare Systems Center Technical Report 1771.

Mann, J.A., Williams, E., Washburn, K. and Grosh, K. (1991). Time-domain analysis of the energy exchange between structural vibrations and acoustic radiation using near-field acoustical holography measurements, *Journal of the Acoustical Society of America*, **90:** 1656-1664.

Marsili, R., Pizzoni, L. and Rossi, G. (2000). Vibration measurements of tools inside fluids by laser doppler techniques: uncertainty analysis, Elsevier Science, Ltd., 2000.

Photiadis, D.M. (1990). The propagation of axisymmetric waves on a fluid-loaded cylindrical shell, *Journal of the Acoustical Society of America*, **88:** 239-250.

Polytech, (2001). *Portable Digital Vibrometer PDV100 User Manual*.

Popper, A. and Hastings, M. (2009). The effects of anthropogenic sources of sound on fish, *Journal of Fish Biology*, **75:** 455-489 <http://www.wsdot.wa.gov/NR/rdonlyres/0B027B4A-F9FF-4C88-8DE0-39B165E4CD94/61427/BA_AnthroSoundonFish.pdf>

Reinhall, G. and Dahl, P.H. (2011). Acoustic radiation from a submerged pile during pile

driving, University of Washington, Seattle, WA.

Robert Miner Dynamic Testing, Inc. (2011). Dynamic pile measurements and analyses, Columbia River Crossing Temporary Pile Test Program.

Shahab, S. and Hastings, M.(2012). Effects of damping on the structural acoustics response of a partially submerged steel pile to an impact force, Inter-noise, New York.

Stokes, A., Cockrell, K., Wilson, J., Davis, D. and Warwick, D. (2010). Mitigation of underwater pile driving noise during offshore construction: final report", technical report to the Department of the Interior Minerals Management Service Report.

Wang, S., Yang, D. and Liu, N. (2007). Investigation of acoustic scale effects and boundary effects for the similitude model of underwater complex shell-structure, *Journal of Marine Science and Application*, **6:** 31-35.

Yang, J. (2007). Spatial coherence in a shallow water waveguide, PhD Dissertation, Georgia Institute of Technology.

Zornig, J.G (1979). Oceanography in underwater acoustics, *Ocean Acoustics*, Edited by J.A. DeSanto, 159-160.